

ELASTIC ANALYSIS OF  
SHEAR TEST PLATE

R. H. Janowski  
M. D. Vanderbilt

Structural Research Report No. 3  
Civil Engineering Department  
Colorado State University  
Fort Collins, Colorado 80521

March, 1970



U18401 0575798

## TABLE OF CONTENTS

	Page
List of Tables . . . . .	vii
List of Figures . . . . .	viii
1. INTRODUCTION . . . . .	1
1.1 Object . . . . .	1
1.2 Scope . . . . .	3
1.3 Acknowledgments . . . . .	4
1.4 Notation . . . . .	5
2. DEVELOPMENT OF PLATE OPERATORS . . . . .	8
2.1 Introductory Remarks . . . . .	8
2.2 Differential Equations for Plates and Beams. . . . .	8
2.3 Finite Difference Operators . . . . .	10
2.4 Newmark Plate Analog Operators . . . . .	16
(a) Moment Operators . . . . .	17
(b) Shear Operators . . . . .	19
(c) Spandrel Beam Operators . . . . .	22
(d) Fictitious Point Operators on the Spandrel Beam . . . . .	23
(e) Fictitious Point Operator at the Corner . . . . .	24
(f) Deflection Operator for Points Adjacent to the Corner of the Column . . . . .	25
(g) Shear Operator at the Corner of the Column . . . . .	30
3. DESCRIPTION OF COMPUTER PROGRAMS . . . . .	34
3.1 Introductory Remarks . . . . .	34
3.2 Description of Program CSUPLT . . . . .	35
3.3 Description of Program SHRMOM . . . . .	36
4. RESULTS . . . . .	37
4.1 Introductory Remarks . . . . .	37
4.2 Deflections. . . . .	38
4.3 Orthogonal Moments . . . . .	40
4.4 Lines of Contraflexure . . . . .	41
4.5 Shear at the Column . . . . .	42
5. SUMMARY, DISCUSSION AND CONCLUSIONS . . . . .	45
5.1 Summary . . . . .	45
5.2 Discussion and Conclusions . . . . .	45

TABLE OF CONTENTS (continued)

	Page
BIBLIOGRAPHY. . . . .	48
TABLES . . . . .	50
FIGURES. . . . .	51
APPENDIX A. SOLUTION OF SIMULTANEOUS EQUATIONS USING THE GAUSS ELIMINATION TECHNIQUE . . . . .	82
A.1 Introductory Remarks . . . . .	82
A.2 Gauss Elimination and Back-Substitution . . . . .	82
A.3 General Description of Algorithm GASTAP for Solving Simultaneous Equations. . . . .	86
A.4 Program CSUPLT--Generation and Solution of the Deflection Equations for the Test Plate . . . . .	88
APPENDIX B. PROGRAM SHRMOM--COMPUTATION OF SHEAR AND MOMENT IN THE TEST PLATE . . . . .	90

## LIST OF TABLES

Table No.		Page
4.1	Equilibrium Check of Shear Forces . . . . .	50

## LIST OF FIGURES

Figure No.		Page
1.1	Reinforced Concrete Test Specimen . . . . .	51
1.2a	Clamped Edge Plate Showing Line of Contraflexure .	52
1.2b	Comparison of Line of Contraflexure in Clamped Plate with Line for Continuous Interior Panel . . .	52
1.3	Mathematical Model of the Test Specimen . . . . .	53
2.1	Plate-Beam Analog at Edge Beam . . . . .	54
2.2	Forces Affecting Equilibrium of Typical Joint in Plate Analog . . . . .	55
2.3	Forces Affecting Equilibrium at Edge Beam Corner Joint in Plate-Beam Analog . . . . .	56
2.4	Forces Affecting Equilibrium of Typical Edge Joint in Plate-Beam Analog. . . . .	57
4.1	Comparison of Deflections on N-S Line of Symmetry for a Specimen with a Point Column . . .	58
4.2	Comparison of Deflections on N-S Line of Symmetry for a Specimen with a 12"x12" Square Column . . . . .	59
4.3	Deflection Curves on N-S Line of Symmetry for a Specimen with a 16"x16" Column and Varied Edge Beam Rigidities . . . . .	60
4.4	Deflection on N-S Line of Symmetry for Specimens with Square Columns . . . . .	61
4.5	Deflection on the Diagonal Line of Symmetry for Specimens with Square Columns . . . . .	62
4.6	Deflection on N-S Line of Symmetry for Specimens with Columns with 16" E-W Dimension and Varying N-S Dimension. . . . .	63

LIST OF FIGURES (continued)

Figure No.		Page
4.7	Deflection on E-W Line of Symmetry for Specimens with Columns with 16" E-W Dimension and Varying N-S Dimension . . . . .	64
4.8	$m_x$ , $m_y$ , $m_{xy}$ on E-W Line of Symmetry for a Specimen with a 16"x16" Column . . . . .	65
4.9	Moment $m_y$ at the Face of the Square Columns in the Test Specimens . . . . .	66
4.10	Moment $m_y$ One Grid Width from the Face of the Square Columns in the Test Specimen . . . . .	67
4.11	Lines of Contraflexure for Principal Moments about Square Columns in the Specimen . . . . .	68
4.12	Lines of Contraflexure Around a 16"x4" Column in the Specimen. . . . .	69
4.13	Lines of Contraflexure Around a 16"x8" Column in the Specimen. . . . .	70
4.14	Lines of Contraflexure Around a 16"x12" Column in the Specimen. . . . .	71
4.15	Lines of Contraflexure Around a 12"x4" Column in the Specimen. . . . .	72
4.16	Lines of Contraflexure Around a 12"x8" Column in the Specimen. . . . .	73
4.17	Lines of Contraflexure Around a 8"x4" Center Column in the Specimen . . . . .	74
4.18	Shear at the Column Face for Square Columns in the Test Plate . . . . .	75
4.19	Shear at One Grid Space $h = L/30$ from Square Columns in the Test Plate . . . . .	76
4.20	Refined Grid Near Column . . . . .	77

LIST OF FIGURES (continued)

Figure No.		Page
4.21	Shear at the Column Face and at $h = L/30$ from the Column Face for the Coarse and Fine Grid . . . . .	78
4.22	Shear at the Column Face for the 16"x4", 16"x8", 16"x12" and 16"x16" Columns in the Test Plate . . .	79
4.23	Shear at One Grid Space from the Column for the 16"x4", 16"x8", 16"x12" and 16"x16" Columns . . .	80
5.1	Continuous Structure More Closely Simulated by the Test Specimen of Fig. 1.1 . . . . .	81
A.1	General Flow Diagram of GASTAP . . . . .	89

## 1. INTRODUCTION

### 1.1 Object

A complete and accurate description of the structural action occurring in the transfer of loads from reinforced concrete flat plate structures to their supporting columns has not yet been obtained. Attempts (4, 5, 6, 8, 9)\* have been made at determining empirical equations which predict the shear strength at the supporting column in flat plates. These equations have been developed on the basis of tests of models which are purported to represent the portion of the plate within the line of contraflexure for the principal moment. As is pointed out by Mowrer and Vanderbilt (10), these test specimens are not truly representative of the structural action of an interior panel of a flat plate with respect to deflections, shears and in-plane forces and more closely resemble footings than continuous structures. Mowrer and Vanderbilt proposed a new type of test specimen (Fig. 1.1) to more closely model the structural action of a continuous flat plate around an interior column.

The reinforced concrete test specimen of Fig. 1.1 was developed after considerations of the elastic model shown in Fig. 1.2a. The elastic plate of Fig. 1.2a is a square, uniformly-loaded plate with clamped edges and a point support at the center. The line of contraflexure for zero principal moments in the clamped plate is

---

\* Numbers in parentheses refer to entries in bibliography.



shown by a dashed line. Shown in Fig. 1.2b are the line of contraflexure from 1.2a and the line of contraflexure for a square, interior, flat plate panel on point supports. An "interior" panel is here defined as a panel which is one of an infinite array of identical panels. In real structures every panel which has at least one continuous panel on each side is closely an "interior" panel.

As is evident in Fig. 1.2b the clamped plate of 1.2a closely models the conditions around an interior column of a continuous flat plate structure. Comparisons of orthogonal moments and deflections show similar agreement. While not shown, studies of a clamped plate having a square column showed similar agreement with a continuous plate on the same size of square columns.

The dimensions of the reinforced concrete test specimen were chosen to model the clamped plate of Fig. 1.2a following a procedure which is described elsewhere (10). As is shown in Chapter 4 the edge beams of the reinforced concrete test structure were not as rigid in torsion as intended and thus the reinforced concrete test specimen does not model the conditions around a column in an interior panel as closely as desired. It does, however, more closely model the structure than do the "footing" type of specimens which have been used in prior studies.

The object of this study is to analytically define the elastic behavior of the test specimen of Fig. 1.1. Main emphasis is on

the determination of shear force distribution at the column and the location of the line of contraflexure about the column.

## 1.2 Scope

The elastic analyses of the specimen were based on the ordinary theory of flexure for beams and plates and were performed using the finite difference method. The Control Data Corporation Model 6400 digital computer at Colorado State University was used to generate and solve the sets of simultaneous finite difference equations which define the deflected surface of the plate. Analyses were performed for several rectangular column sizes and for different edge beam torsional and flexural rigidities.

The mathematical model shown in Fig. 1.3 was used in the analyses of the test specimen. The edge beam in the model is assumed to be a line beam. The neutral axis of the edge beam is assumed to be in the plane of the neutral surface of the plate in order to preclude consideration of tee-beam action. Torsion in the beam is assumed uniform between node points. Non-deflecting point supports are located at each of the four corners of the plate and the center column is assumed rigid. The plate is loaded perpendicular to the plane of the plate with uniform load  $q$ .

A solution for the plate deflection is obtained by first setting up a square grid on the plate. At each node point on the

grid an operator form of the governing differential equation is written which describes the deflection at the node point in terms of the deflections at surrounding node points. The solution of the simultaneous set of difference equations for all the node points on the grid yields the deflection of each node point. Using these deflections, moments and shears in the specimen are computed.

Results of the analyses include deflections for the total plate; shear force distribution around the column; the orthogonal moments  $m_x$  and  $m_y$ , the twisting moment  $m_{xy}$ , and the maximum principal moments; and the location of the lines of contraflexure around the column.

Chapter 2 contains a discussion of the plate operators used and Chapter 3 contains a description of the computer programs used in the analyses. The effect of varying the beam rigidity and column size on the deflections, shears, and moments in the plate are discussed in Chapter 4. Chapter 5 contains the summary and conclusions. Appendices A and B are a more detailed discussion of the computer programs.

### 1.3 Acknowledgments

This report was prepared as a Master's Thesis under the direction of Dr. M.D. Vanderbilt, Associate Professor of Civil Engineering. Financial support for the project was a grant by the National Science Foundation.

### 1.4 Notation

The following notation is used in this thesis.

a = width of beam

b = depth of beam

C =  $a^3 b (1 - 0.63 \frac{a}{b})$   
 a measure of the torsional rigidity of a beam cross-section

D =  $\frac{E_s I_s}{(1 - \mu^2)} = \frac{E_s t^3}{12 (1 - \mu^2)}$

$E_b$  = modulus of elasticity of the beam material

$E_s$  = modulus of elasticity of the slab material

G =  $\frac{E_b}{2(1 + \mu)}$  = shear modulus of elasticity of the beam material

h = distance between node points

H =  $\frac{E_b I_b}{2DL}$  = ratio of beam flexural stiffness to plate stiffness

H' =  $\frac{E_b I_b}{Dh}$  = a measure of the flexural stiffness of a beam

$I_b$  = moment of inertia of the cross-section of a beam

$I_s$  =  $\frac{t^3}{12}$  = moment of inertia per unit width of plate

$J$	=	$\frac{GC}{2DL}$ = ratio of beam torsional stiffness to plate stiffness
$J'$	=	$\frac{GC}{Dh}$ = a measure of the torsional stiffness of a beam
$L$	=	half the length of the side on the mathematical model (Fig. 1.3)
$m$	=	bending or twisting moment per unit width of plate
$m_{\max}$	=	maximum principal moment
$\bar{m}$	=	bending or twisting moment on a grid width of plate $h$ $\bar{m} = mh$
$\bar{m}$	=	bending or twisting moment acting on a width of plate $h/2$ $\bar{m}' = \frac{\bar{m}}{2} = \frac{mh}{2}$
$M$	=	bending moment in a beam
$n$	=	number of node points or deflection equations
$q$	=	uniformly distributed load per unit of area
$Q$	=	total load acting at a node point
$R$	=	plate reaction
$t$	=	thickness of the plate
$T$	=	torsional moment in a beam
$v$	=	vertical shear per unit width of plate
$\bar{v}$	=	vertical shear acting on a width of plate of $h$ $\bar{v} = vh$
$\bar{v}'$	=	vertical shear acting on a width of plate of $h/2$

$V$	=	vertical shear in a beam
$w$	=	deflection of the plate, positive downward
$x, y, z$	=	rectangular reference coordinates
$\mu$	=	Poisson's ratio

## 2. DEVELOPMENT OF PLATE OPERATORS

### 2.1 Introductory Remarks

The ordinary theory of flexure of beams and flat plates was assumed to describe the structural action of the specimen and is discussed in section 2.2. The analyses were accomplished using both the calculus of finite differences which is discussed in section 2.3 and the Newmark plate analog which is discussed in section 2.4. Presentation and derivation of all operators used in the analyses are included in this chapter.

### 2.2 Differential Equations for Plates and Beams

Following is a list of differential equations for medium thick plates and beams. Complete derivation of the plate equations is found in Timoshenko (14) and the beam equations derivations are given by Timoshenko (15).

The governing differential equation for plates is

$$\frac{\partial^4 w}{\partial x^4} + \frac{2\partial^4 w}{\partial x^2 \partial y^2} + \frac{\partial^4 w}{\partial y^4} = \frac{q}{D} \quad (2.1)$$

The bending moments, twisting moments, shears and reactions are related to the deflections by the following equations.

$$m_x = -D \left( \frac{\partial^2 w}{\partial x^2} + \mu \frac{\partial^2 w}{\partial y^2} \right) \quad (2.2)$$

$$m_y = -D \left( \frac{\partial^2 w}{\partial y^2} + \mu \frac{\partial^2 w}{\partial x^2} \right) \quad (2.3)$$

$$m_{xy} = -D(1-\mu) \left( \frac{\partial^2 w}{\partial x \partial y} \right) \quad (2.4)$$

$$v_x = \frac{\partial m_x}{\partial x} + \frac{\partial m_{xy}}{\partial y} = -D \left( \frac{\partial^3 w}{\partial x^3} + \frac{\partial^3 w}{\partial x \partial y^2} \right) \quad (2.5)$$

$$v_y = \frac{\partial m_y}{\partial y} + \frac{\partial m_{xy}}{\partial x} = -D \left( \frac{\partial^3 w}{\partial y^3} + \frac{\partial^3 w}{\partial y \partial x^2} \right) \quad (2.6)$$

$$R_x = v_x + \frac{\partial m_{xy}}{\partial y} = -D \left( \frac{\partial^3 w}{\partial x^3} + 2 \frac{\partial^3 w}{\partial x \partial y^2} \right) \quad (2.7)$$

$$R_y = v_y + \frac{\partial m_{xy}}{\partial x} = -D \left( \frac{\partial^3 w}{\partial y^3} + 2 \frac{\partial^3 w}{\partial y \partial x^2} \right) \quad (2.8)$$

The fundamental equations of beam flexure are:

$$q = -E_b I_b \frac{d^4 w}{dx^4} \quad (2.9)$$

$$V_x = -E_b I_b \frac{d^3 w}{dx^3} \quad (2.10)$$

$$M_x = -E_b I_b \frac{d^2 w}{dx^2} \quad (2.11)$$

$$T = -CG \frac{d}{dx} \left( \frac{dw}{dy} \right) \quad (2.12)$$

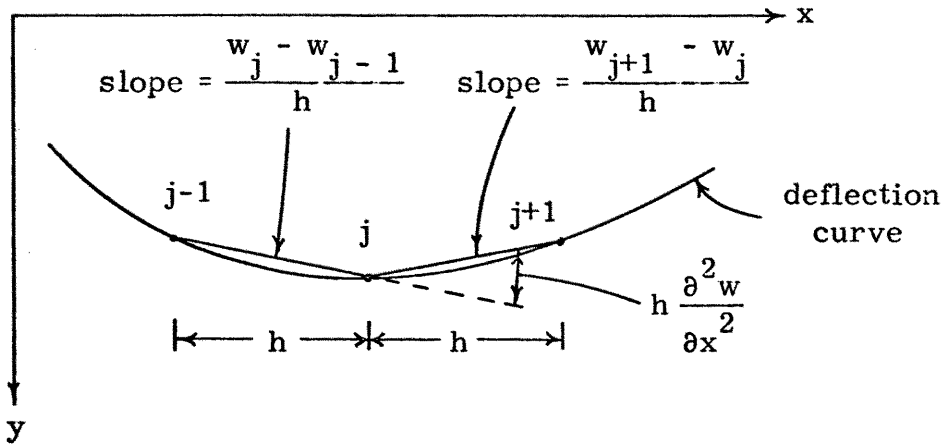
A solution of the governing equation for the deflection  $w$  which satisfies given boundary conditions for the plate will lead to the solution of shears and moments in the plate through the use of the above equations.



### 2.3 Finite Difference Operators

The calculus of finite differences was used to derive the operator forms of the differential equations at interior points on the specimen where the plate is continuous and no difficult boundary conditions exist. Following is the basic theory of finite differences and the derivation of basic operator forms as well as those used in the analyses.

The illustration below shows the deflected shape of what may be a beam or a cross-section view of a plate in the x-y plane. The deflected shape is approximated by straight lines between node points spaced at  $h$ .



$$\text{The average slope at } j = \frac{[w_{j+1} - w_j] + [w_j - w_{j-1}]}{2h}$$

$$= \frac{1}{2h} [-w_{j-1} + w_{j+1}] \quad (2.13)$$

The average slope at  $j$  in operator form is

$$\frac{\partial w}{\partial x} = \frac{1}{2h} \left[ \begin{array}{c} -1 \\ | \\ j-1 \end{array} \text{---} \begin{array}{c} 0 \\ | \\ j \end{array} \text{---} \begin{array}{c} +1 \\ | \\ j+1 \end{array} \right] w. \quad (2.14)$$

The curvature at point  $j$  is obtained by operating on equation 2.14.

$$h \frac{\partial}{\partial x} \left( \frac{\partial w}{\partial x} \right) = h \frac{\partial^2 w}{\partial x^2} = \frac{[w_{j+1} - w_j][w_j - w_{j-1}]}{h} \quad (2.15)$$

$$\frac{\partial^2 w}{\partial x^2} = \frac{1}{h^2} \left[ \begin{array}{c} 1 \\ | \\ j-1 \end{array} \text{---} \begin{array}{c} -2 \\ | \\ j \end{array} \text{---} \begin{array}{c} 1 \\ | \\ j+1 \end{array} \right] w \quad (2.16)$$

Similarly the third and fourth order operators are derived.

$$\frac{\partial}{\partial x} \left( \frac{\partial^2 w}{\partial x^2} \right) = \frac{\partial^3 w}{\partial x^3} = \frac{1}{2h^3} \left[ \begin{array}{c} -1 \\ | \\ j-2 \end{array} \text{---} \begin{array}{c} 2 \\ | \\ j-1 \end{array} \text{---} \begin{array}{c} 0 \\ | \\ j \end{array} \text{---} \begin{array}{c} -2 \\ | \\ j+1 \end{array} \text{---} \begin{array}{c} 1 \\ | \\ j+2 \end{array} \right] w \quad (2.17)$$

$$\frac{\partial}{\partial x} \left( \frac{\partial^3 w}{\partial x^3} \right) = \frac{\partial^4 w}{\partial x^4} = \frac{1}{h^4} \left[ \begin{array}{c} 1 \\ | \\ j-3 \end{array} \text{---} \begin{array}{c} -4 \\ | \\ j-2 \end{array} \text{---} \begin{array}{c} 6 \\ | \\ j-1 \end{array} \text{---} \begin{array}{c} -4 \\ | \\ j \end{array} \text{---} \begin{array}{c} 1 \\ | \\ j+1 \end{array} \right] w \quad (2.18)$$

Similar operators in the  $y$  direction are obtained as above.

$$\frac{\partial w}{\partial y} = \frac{1}{2h} \left[ \begin{array}{c} 1 \\ | \\ j+1 \end{array} \text{---} \begin{array}{c} 0 \\ | \\ j \end{array} \text{---} \begin{array}{c} -1 \\ | \\ j-1 \end{array} \right] w \quad (2.19)$$

$$\frac{\partial^2 w}{\partial y^2} = \frac{1}{h^2} \left[ \begin{array}{c} 1 \\ -2 \\ 1 \end{array} \right] w \quad (2.20)$$

$$\frac{\partial^3 w}{\partial y^3} = \frac{1}{2h^3} \left[ \begin{array}{c} 1 \\ -2 \\ 0 \\ 2 \\ -1 \end{array} \right] w \quad (2.21)$$

$$\frac{\partial^4 w}{\partial y^4} = \frac{1}{h^4} \left[ \begin{array}{c} 1 \\ -4 \\ 6 \\ -4 \\ 1 \end{array} \right] w \quad (2.22)$$

$$\frac{\partial^2}{\partial x^2} \left( \frac{\partial^2 w}{\partial y^2} \right) = \frac{\partial^4 w}{\partial x^2 \partial y^2} = \frac{1}{h^4} \begin{bmatrix} | & & | \\ \hline 1 & -2 & 1 \\ \hline | & \bullet & | \\ \hline -2 & 4 & -2 \\ \hline | & & | \\ \hline 1 & -2 & 1 \\ \hline \end{bmatrix} w \quad (2.23)$$

Now referring to the governing differential equation

$$\frac{\partial^4 w}{\partial x^4} + 2 \frac{\partial^4 w}{\partial x^2 \partial y^2} + \frac{\partial^4 w}{\partial y^4} = \frac{q}{D} \quad (2.1)$$

the first term is expressed by operator (2.18); the second term is expressed by operator (2.23) multiplied by two; and the third term is expressed by operator (2.22). Summing the three equations and multiplying both sides by  $h^4$  results in equation (2.24), the general 13 point deflection operator for plates.

$$\begin{bmatrix} | & & & & | \\ \hline & & 1 & & \\ \hline & & | & & \\ \hline & 2 & -8 & 2 & \\ \hline & | & & | & \\ \hline | & -8 & 20 & -8 & | \\ \hline & | & & | & \\ \hline & 2 & -8 & 2 & \\ \hline & & | & & \\ \hline & & 1 & & \\ \hline \end{bmatrix} w = \frac{qh^4}{D} \quad (2.24)$$

Using the above derived operators and the fundamental equations for the flexure of plates the following operators may be derived.

$$m_x = -D \left( \frac{\partial^2 w}{\partial x^2} + \mu \frac{\partial^2 w}{\partial y^2} \right)$$

$$= \frac{D}{h^2} \left[ \begin{array}{ccc} & & -\mu \\ & & | \\ & & | \\ -1 & & 2+2\mu & & -1 \\ & & | \\ & & | \\ & & -\mu \end{array} \right] w \quad (2.25)$$

$$m_y = -D \left( \frac{\partial^2 w}{\partial y^2} + \mu \frac{\partial^2 w}{\partial x^2} \right)$$

$$= \frac{D}{h^2} \left[ \begin{array}{ccc} & & -1 \\ & & | \\ & & | \\ -\mu & & 2+2\mu & & -\mu \\ & & | \\ & & | \\ & & -1 \end{array} \right] w \quad (2.26)$$

$$m_{xy} = -D (1-\mu) \left( \frac{\partial^2 w}{\partial x \partial y} \right)$$

$$= \frac{D}{h^2} \frac{1-\mu}{4} \left[ \begin{array}{c|c|c} 1 & & -1 \\ \hline & \bullet & \\ \hline -1 & & +1 \end{array} \right] w \quad (2.27)$$

$$v_x = -D \left( \frac{\partial^3 w}{\partial x^3} + \frac{\partial^3 w}{\partial x \partial y^2} \right) = -D \frac{\partial w}{\partial x} \left( \frac{\partial^2 w}{\partial x^2} + \frac{\partial^2 w}{\partial y^2} \right)$$

$$= \frac{D}{2h^3} \left[ \begin{array}{c|c|c} -1 & 0 & +1 \\ \hline -1 & +4 & -4 & +1 \\ \hline & -1 & 0 & +1 \end{array} \right] w \quad (2.28)$$

$$v_y = -D \left( \frac{\partial^3 w}{\partial y^3} + \frac{\partial^3 w}{\partial y \partial x^2} \right) = -D \frac{\partial w}{\partial y} \left( \frac{\partial^2 w}{\partial y^2} + \frac{\partial^2 w}{\partial x^2} \right)$$

$$= \frac{D}{2h^3} \begin{bmatrix} & & & & & \\ & & & & & \\ & & +1 & & & \\ & +1 & & -4 & & +1 \\ & 0 & & 0 & & 0 \\ & -1 & & +4 & & -1 \\ & & & & & \\ & & & & & -1 \\ & & & & & \end{bmatrix} w \quad (2.29)$$

#### 2.4 Newmark Plate Analog Operators

The above operators have been easily derived using the calculus of finite differences. For more difficult operators involving discontinuities or special boundary conditions a model called Newmark's plate analog is more conveniently used (11). Figure 2.1 shows the plate analog. It is composed of rigid bars connecting elastic hinges, with torsion springs connecting parallel bars. The following are characteristics of the analogous plate.

1. The bars are weightless and rigid.
2. The mass of the plate and external loads are concentrated at the hinges.
3. The resultant of direct stresses are bending moments acting at the elastic hinges and at the ends of each bar.
4. The resultant of the vertical shearing stresses are shearing forces acting at the elastic hinges and at the ends of each bar.
5. The resultant of the horizontal shearing stresses are twisting moments concentrated in the torsion springs.

The form of the equations governing deflections of the model are exactly the same as the finite difference form of the governing fourth order differential equation from the theory of flexure of plates.

The operators obtained using the plate analog are described below.

(a) Moment Operators

$\bar{m}_{ox}$  and  $\bar{m}_{oy}$  are the same form as  $m_x$  and  $m_y$  obtained by finite difference calculus. Referring to Fig. 2.2,  $\bar{m}_{ox}$  and  $\bar{m}_{oy}$  are given by the expressions

$$\bar{m}_{ox} = \frac{D}{h} \left[ \begin{array}{c} \begin{array}{ccc} & & -\mu \\ \hline & & \\ \hline -1 & \bullet & 2+2\mu & -1 \\ \hline & & \\ \hline & & -\mu \\ & & \end{array} \\ w \end{array} \right] \quad (2.30)$$

$$\bar{m}_{oy} = \frac{D}{h} \left[ \begin{array}{c} \begin{array}{ccc} & & -1 \\ \hline & & \\ \hline -\mu & \bullet & 2+2\mu & -\mu \\ \hline & & \\ \hline & & -1 \\ & & \end{array} \\ w \end{array} \right] \quad (2.31)$$



$\frac{-B}{m_{xy}}$  is of the same form as  $m_{xy}$  from the finite difference calculus, but it is applied to obtain the torsion in the torsion springs in quadrant B of Fig. 2.2 instead of the torsion at joint o. The torsional moment operators for the four quadrants around joint o are given below.

$$\frac{-B}{m_{xy}} = \frac{D}{h} \quad \left[ \begin{array}{c} \text{joint o} \\ \begin{array}{|c|c|} \hline 1-\mu & -1+\mu \\ \hline \end{array} \\ \text{B} \\ \begin{array}{|c|c|} \hline -1+\mu & 1-\mu \\ \hline \end{array} \\ w \end{array} \right] \quad (2.32)$$

$$\frac{-A}{m_{xy}} = \frac{D}{h} \quad \left[ \begin{array}{c} \begin{array}{|c|c|} \hline 1-\mu & -1+\mu \\ \hline \end{array} \\ \text{A} \\ \begin{array}{|c|c|} \hline -1+\mu & 1-\mu \\ \hline \end{array} \\ \text{joint o} \\ w \end{array} \right] \quad (2.33)$$

$$\frac{-C}{m_{xy}} = \frac{D}{h} \quad \left[ \begin{array}{c} \begin{array}{|c|c|} \hline 1-\mu & -1+\mu \\ \hline \end{array} \\ \text{C} \\ \begin{array}{|c|c|} \hline -1+\mu & 1-\mu \\ \hline \end{array} \\ \text{joint o} \\ w \end{array} \right] \quad (2.34)$$

$$\frac{-D}{m_{xy}} = \frac{D}{h} \quad \left[ \begin{array}{c} \begin{array}{|c|c|} \hline 1-\mu & -1+\mu \\ \hline \end{array} \\ \text{D} \\ \begin{array}{|c|c|} \hline -1+\mu & 1-\mu \\ \hline \end{array} \\ \text{joint o} \\ w \end{array} \right] \quad (2.35)$$

(b) Shear Operators

The shear operator is derived using Fig. 2.2 as follows. The sum of the moments about end n of bar on is equal to zero.

$$(\bar{v}_{on})(h) + \bar{m}_{oy} - \bar{m}_{ny} + \bar{m}_{xy}^D - \bar{m}_{xy}^A = 0 \quad (2.36)$$

$$\bar{v}_{on} = \frac{1}{h} ( -\bar{m}_{oy} + \bar{m}_{ny} - \bar{m}_{xy}^D + \bar{m}_{xy}^A ) \quad (2.37)$$

Substituting the operator forms of the terms on the right side of equation (2.37) gives

$$\bar{v}_{on} = \frac{D}{h^2} \begin{bmatrix} & & & -1 & & \\ & & & & & \\ -1 & & & 5 & & -1 \\ | & & & & & | \\ 1 & & & -5 & & 1 \\ | & & & & & | \\ & & & & & \\ & & & & & 1 \\ & & & & & | \end{bmatrix} w \quad (2.38)$$

and similarly

$$\bar{v}_{ow} = \frac{D}{h^2} \begin{bmatrix} & & & 1 & & -1 \\ & & & & & \\ 1 & & & -5 & & 5 \\ | & & & & & | \\ & & & & & -1 \\ | & & & & & | \\ & & & 1 & & -1 \\ & & & & & | \end{bmatrix} w \quad (2.39)$$

$$\bar{v}_{oe} = \frac{D}{h^2} \left[ \begin{array}{c} \begin{array}{cc} 1 & -1 \\ -5 & +5 \\ 1 & -1 \end{array} \\ \begin{array}{c} 1 \\ -1 \end{array} \end{array} \right] w \quad (2.40)$$

$$\bar{v}_{os} = \frac{D}{h^2} \left[ \begin{array}{c} \begin{array}{cc} -1 & -1 \\ 5 & -5 \\ 1 & 1 \end{array} \\ \begin{array}{c} -1 \\ 1 \end{array} \end{array} \right] w \quad (2.41)$$

The operators for the beam shear at the northwest corner support are derived as follows from Fig. 2.3.

To obtain  $V_{oe}$  at the corner set the sum of the moments about end e of bar oe equal to zero.

$$(V_{oe})(h) + (\bar{v}'_{oe})(h) + M_{ox} + \bar{m}'_{ox} + \bar{m}_{xy}^B - M_{ex} - \bar{m}'_{ex} = 0 \quad (2.42)$$

$$V_{oe} = -v'_{oe} - \frac{M_{ox}}{h} - \frac{\bar{m}'_{ox}}{h} - \frac{\bar{m}_{xy}^B}{h} + \frac{M_{ex}}{h} + \frac{\bar{m}'_{ex}}{h} \quad (2.43)$$

Substituting the operator forms of the terms on the right side of equation (2.43) gives

$$V_{oe} = \frac{D}{h^2} \left[ \begin{array}{c|c|c} \frac{1+\mu}{2} & \frac{1-\mu}{2} & \\ \hline H' & -3H' & 3H' & -H' \\ \hline \frac{1-\mu}{2} & -\frac{1+\mu}{2} & \\ \hline \end{array} \right] w \quad (2.44)$$

To obtain  $V_{os}$  the sum of the moments about end s of bar os is set equal to zero.

$$(V_{os})(h) + (\bar{v}'_{os})(h) - M_{oy} - \bar{m}'_{oy} - \frac{\bar{m}^B}{h} + M_{oy} + \bar{m}'_{sy} = 0 \quad (2.45)$$

$$V_{os} = -\bar{v}'_{os} + \frac{M_{oy}}{h} + \frac{\bar{m}'_{oy}}{h} + \frac{\bar{m}^B}{h} - \frac{M_{sy}}{h} - \frac{\bar{m}'_{sy}}{h} \quad (2.46)$$

Substituting the operator forms of the terms on the right side of equation (2.46) gives

$$V_{os} = \frac{D}{h^2} \left[ \begin{array}{c|c|c} & & -H' \\ \hline \frac{1-\mu}{2} & 3H' & \frac{1+\mu}{2} \\ \hline \frac{1+\mu}{2} & -3H' & \frac{1-\mu}{2} \\ \hline & & H' \end{array} \right] w. \quad (2.47)$$

(c) Spandrel Beam Operators

The deflection operator for an edge beam is found as follows:

Referring to Fig. 2.4 the vertical forces at joint o are summed giving

$$(V_{oe} + \bar{v}'_{oe}) - \bar{v}_{os} - (V_{ow} + \bar{v}'_{ow}) + Q = 0. \quad (2.48)$$

Next moments about end e of bar oe are summed giving

$$(V_{oe} + \bar{v}'_{oe})h + M_{ox} + \bar{m}'_{ox} + \bar{m}_{xy}^B - M_{ex} - \bar{m}'_{ex} = 0 \quad (2.49)$$

which reduces to

$$(V_{oe} + \bar{v}'_{oe}) = + \frac{1}{h} ( -M_{ox} - \bar{m}'_{ox} - \bar{m}_{xy}^B + M_{ex} + \bar{m}'_{ex} ). \quad (2.50)$$

A summation of moments about end w of bar ow gives

$$(V_{ow} + \bar{v}'_{ow})h + M_{wx} + \bar{m}'_{wx} + \bar{m}_{xy}^C - M_{ox} - \bar{m}'_{ox} = 0 \quad (2.51)$$

which reduces to

$$(V_{ow} + \bar{v}'_{ow}) = + \frac{1}{h} ( -M_{wx} - \bar{m}'_{wx} - \bar{m}_{xy}^C + M_{ox} + \bar{m}'_{ox} ). \quad (2.52)$$

Now substitution of equation (2.50) and equation (2.52) into equation (2.43) leads to

$$\begin{aligned} \frac{1}{h} (-M_{ox} - \bar{m}'_{ox} - \bar{m}_{xy}^B + M_{ex} + \bar{m}'_{ex}) - \bar{v}_{os} - \frac{1}{h} (-M_{wx} - \bar{m}'_{wx} \\ - \bar{m}_{xy}^C + M_{ox} + \bar{m}'_{ox}) + Q = 0 \end{aligned} \quad (2.53)$$

which may be rewritten as

$$\begin{aligned} & \frac{2}{h} M_{ox} - \frac{2}{h} m_{ox} - \frac{\bar{m}_{xy}^B}{h} + \frac{M_{ex}}{h} + \frac{\bar{m}'_{ex}}{h} + \frac{M_{wx}}{h} + \frac{\bar{m}'_{wx}}{h} \\ & + \frac{\bar{m}_{xy}^C}{h} - \bar{v}'_{os} + Q = 0. \end{aligned} \tag{2.54}$$

Finally the substitution of the operator forms of the terms in equation (2.54) gives the following deflection operator for the edge beam.

$$\left[ \begin{array}{ccccc} & \frac{\mu}{2} & -(1+\mu) & \frac{\mu}{2} & \\ \frac{1}{2} + H' & -(4+4H') & (10+6H') & -(4+4H') & (\frac{1}{2}+H') \\ & 2\frac{\mu}{2} & -7+\mu & 2\frac{\mu}{2} & \\ & & 1 & & \end{array} \right] w = \frac{Qh^2}{D} \tag{2.55}$$

(d) Fictitious Point Operators on the Spandrel Beam

Following is the derivation of the operator which provides the additional equations necessary for the fictitious points.

The operator is derived from the equation expressing equilibrium of moments about the axis of the edge beam in Fig. 2.4.

$$T_{ow} - T_{oe} + \bar{m}_{oy} = 0 \quad (2.56)$$

$$T_{ow} = \frac{J'D}{2h} (-w_{sw} + w_{nw} + w_s - w_n) \quad (2.57)$$

$$T_{oe} = \frac{J'D}{2h} (-w_s + w_n + w_{se} - w_{ne}) \quad (2.58)$$

Substituting the operator forms of the terms in equation (2.56) and dividing by  $\frac{D}{2h}$  gives equation (2.59).

$$\left[ \begin{array}{ccc} J' & -2(J'+1) & J' \\ -2\mu & 4(1+\mu) & -2\mu \\ -J' & 2(J'-1) & -J' \end{array} \right] w = 0 \quad (2.59)$$

beam

This equation is applied at every node point on the edge beam (except at the corner) to provide the necessary extra equations for determining the deflections of the points outside the plate.

#### (e) Fictitious Point Operator at the Corner

Following is a derivation of the fictitious point operators at the corner of the slab.

Set the summation of torque about the x axis at the corner joint equal to zero in Fig. 2.3.

$$M_{oy} + \bar{m}'_{oy} - T_{oe} = 0 \quad (2.60)$$

Substituting the operator forms of the terms in equation (2.60) gives

$$\left[ \begin{array}{c}
 \left[ \begin{array}{ccc}
 & -H' - \frac{1}{2} \frac{J'}{2} + \frac{J'}{2} & \\
 \frac{\mu}{2} & 2H' + 1 + \mu & \frac{\mu}{2} \\
 \text{corner} & & \\
 & -H' - \frac{1}{2} \frac{J'}{2} & \frac{J'}{2}
 \end{array} \right]
 \end{array} \right] w = 0. \quad (2.61)$$

Similarly torsion about y at the corner joint = 0.

$$M_{ox} + \bar{m}'_{ox} + T_{os} = 0 \quad (2.62)$$

Substituting the operator forms of the terms in equation (2.62) gives

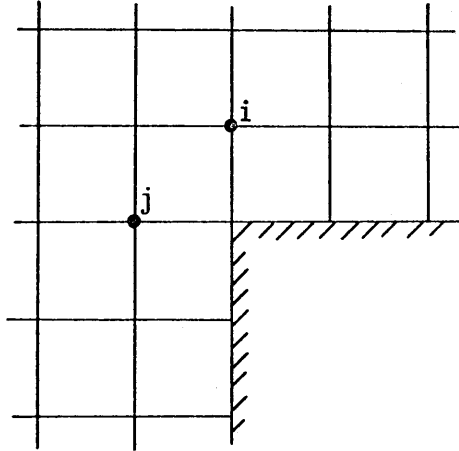
$$\left[ \begin{array}{c}
 \left[ \begin{array}{ccc}
 & -\frac{\mu}{2} & \\
 -H' - \frac{1}{2} \frac{J'}{2} & 2H' + 1 + \mu & -H' - \frac{1}{2} \frac{J'}{2} \\
 \text{corner} & & \\
 \frac{J'}{2} & -\frac{\mu}{2} & \frac{J'}{2}
 \end{array} \right]
 \end{array} \right] w = 0. \quad (2.63)$$

(f) Deflection Operator for Points Adjacent to the Corner of the Column

The corner of the column is a peculiar boundary because it is essentially the orthogonal intersection of two clamped edges. The 13 point deflection operator for plates may not be simply applied at grid points adjacent to the column corner (i and j in figure below) using



the usual technique of reflecting operator values across clamped edge boundaries. The operator must be broken into its component parts and specially derived for these grid points.



Following is the derivation of the deflection operators at the two grid points  $i$  and  $j$ .

Using Fig. 2.2 as a reference set the summation of vertical forces on joint  $o$  equal to zero.

$$\bar{v}_{ow} + \bar{v}_{os} - \bar{v}_{on} - \bar{v}_{oe} - Q = 0 \quad (2.64)$$

Or solving for  $Q$

$$Q = \bar{v}_{ow} + \bar{v}_{os} - \bar{v}_{on} - \bar{v}_{oe} . \quad (2.65)$$

Now obtain the operator form for all terms on the right hand side of equation (2.65). The general operator form for  $\bar{v}_{on}$  is derived for equation (2.38) and the operator forms for  $\bar{v}_{ow}$ ,  $\bar{v}_{os}$  and  $\bar{v}_{oe}$  and



$$v_{oe} = \frac{1}{h} (-\bar{m}_{ox} + \bar{m}_{ex} - \bar{m}_{xy}^B + \bar{m}_{xy}^A) \quad (2.70)$$

$$= \frac{D}{h^2} \begin{bmatrix} & & 1 & -1 \\ +1 & -5 & +5 & -1 \\ & & & & & \end{bmatrix} w \quad (2.71)$$

$$\bar{v}_{ow} = \frac{1}{h} (+\bar{m}_{ox} - \bar{m}_{wx} - \bar{m}_{xy}^C + \bar{m}_{xy}^D) \quad (2.72)$$

$$= \frac{D}{h^2} \begin{bmatrix} & & 1 & -1 \\ 1 & -5 & 5 & -1 \\ & & & & & \end{bmatrix} w \quad (2.73)$$

Substitution of equations (2.67), (2.69), (2.71) and (2.73) into equation (2.65) results in the deflection operator (2.74) at the points adjacent to the column.

$$\left[ \begin{array}{cccc}
 & & +1 & \\
 & 2 & -8 & 2 \\
 +1 & -8 & 21 & -8 & +1 \\
 & 2+\mu & & & \\
 & & & & 
 \end{array} \right] w = \frac{qh^4}{D} \quad (2.74)$$

A similar equation results for the other point adjacent to the corner of the column and is given as equation (2.75)

$$\left[ \begin{array}{ccc}
 & +1 & \\
 & 2 & -8 & 2+\mu \\
 +1 & -8 & 21 & \\
 & 2 & -8 & \\
 & & +1 & 
 \end{array} \right] w = \frac{qh^4}{D} \quad (2.75)$$

(g) Shear Operator at the Corner of the Column

The determination of shear force at the column corner requires special forms of the shear operators  $\bar{v}_{on}$  and  $\bar{v}_{ow}$ . These special operators are the result of the peculiar boundary condition at the corner of the column which is essentially the orthogonal intersection of two clamped edges.

Following is the derivation of the shear operator  $\nabla_{on}$  at the column corner. Referring to section (b) of Chapter 2 the shear  $\bar{v}_{on}$  is

$$\bar{v}_{on} = \frac{1}{h} (-\bar{m}_{oy} + \bar{m}_{ny} - \bar{m}_{xy}^D + \bar{m}_{xy}^A). \quad (2.37)$$

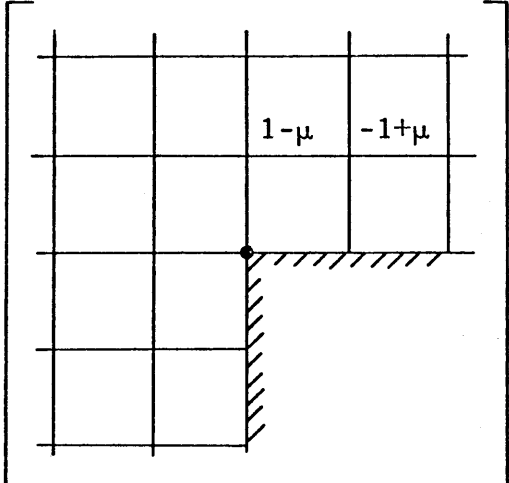
The operator forms of the terms on the right side of the equation are given below.

$$\bar{m}_{oy} = \frac{D}{h} \left[ \begin{array}{c} \begin{array}{cccc} | & | & | & | \\ | & | & | & | \\ | & | & | & | \\ | & | & | & | \\ | & | & | & | \end{array} \\ \begin{array}{c} -2 \\ -2\mu \end{array} \end{array} \right] w \quad (2.76)$$

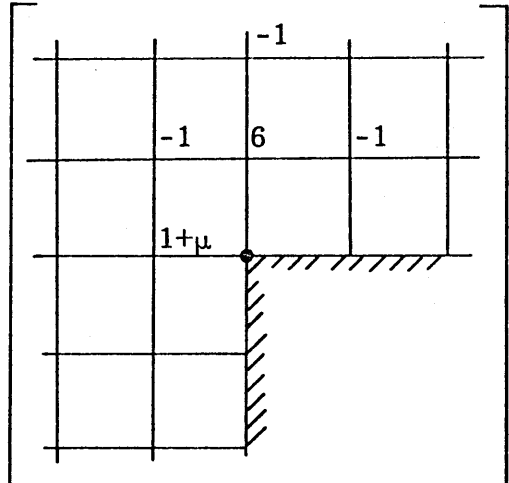
The diagram shows a 4x4 grid of nodes. The right edge and the bottom edge are fixed, indicated by hatching. The corner node (bottom-right) is labeled  $-2\mu$ . The node immediately to its right is labeled  $-2$ . The grid is enclosed in large square brackets, and the letter  $w$  is placed to the right of the brackets.

$$\bar{m}_{ny} = \frac{D}{h} \left[ \begin{array}{cccc} & & -1 & \\ & & & \\ & -\mu & 2+2\mu & -\mu \\ & & & \\ & & & \\ & & & \\ & & & \end{array} \right] w \quad (2.77)$$

$$\bar{m}_{xy} = \frac{D}{h} \left[ \begin{array}{cccc} & & & \\ & & & \\ & 1-\mu & -1+\mu & \\ & & & \\ & & & \\ & & & \\ & -1+\mu & & \\ & & & \\ & & & \end{array} \right] w \quad (2.78)$$

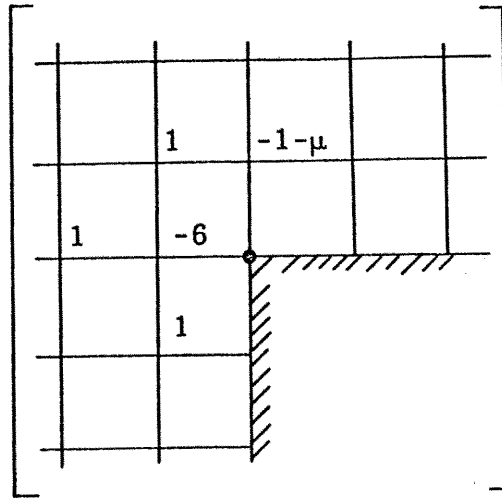
$$\frac{-A}{m_{xy}} = \frac{D}{h} \quad (2.79)$$


Substitution of equations (2.76), (2.77), (2.78) and (2.79) into equation (2.37) gives the shear operator  $\bar{v}_{on}$  at the corner of the column.

$$\bar{v}_{on} = \frac{D}{h^2} \quad (2.80)$$


The operator for  $\bar{v}_{ow}$  at the column corner is derived in a similar manner and is given below in equation (2.81).

$$\bar{v}_{ow} = \frac{D}{h^2}$$



w

(2.81)



### 3. DESCRIPTION OF COMPUTER PROGRAMS

#### 3.1 Introductory Remarks

The analyses of the test structures required the solution of from 997 to 1021 simultaneous finite difference deflection equations of the form

$$\begin{bmatrix} C \\ \text{nxn} \end{bmatrix} \begin{bmatrix} w \\ \text{nx1} \end{bmatrix} = \begin{bmatrix} K \\ \text{nx1} \end{bmatrix} \frac{qL^4}{D} \quad (3.1)$$

where

C = the coefficient matrix formed by the plate operators

w = the plate deflection vector

K = the load term or constant vector

n = number of node points

Row i of matrix equation (3.1) is the difference equation describing the deflection of point i in terms of the deflections of the node points surrounding node point i. Due to the node point numbering scheme (Appendix A) and the form of the deflection operators, C is a banded matrix with a band width of 129, with 64 elements on either side of the main diagonal. All elements outside the band are zero. Due to the boundary conditions, the band is not symmetrical nor is the matrix well conditioned.

To cope with the problems of non-symmetry and ill-conditioning in the coefficient matrix a Gauss elimination procedure combined with back-substitution was used as the equation solution

technique. Program CSUPLT generates and solves the deflection equations for test plates with various sized rectangular columns. Program SHRMOM then uses the deflections obtained from CSUPLT to compute shears and moments in the plate.

Both programs are written in FORTRAN EXTENDED for use with the SCOPE operating system on the Control Data Corporation Model 6400 digital computer at Colorado State University. The two programs are described briefly below and in detail in the appendices.

### 3.2 Description of Program CSUPLT

Program CSUPLT computes the deflections of the test specimen for various column sizes, spandrel beam torsional rigidities and spandrel beam flexural rigidities.

The square plate with a rectangular column is symmetrical about an east-west and a north-south line through the column (Fig. 1.3). Therefore, only one quadrant of the plate must be analyzed to describe the action of the whole plate. The north-west quadrant was selected for the analyses. This quarter of the plate was divided with a 30x30 grid plus one fictitious grid line along each outside edge making a total grid size of 31x31 (Fig. 1.3). The node points are numbered consecutively west to east and north to south with the variation in column size affecting node point numbering on east-west grid lines which intercept the column. The program

generates a deflection equation for each node point and then a Gauss elimination, back-substitution technique is used to solve the equations for the plate deflections. These deflections along with dimensionless parameters defining the geometry of the plate and the node point numbering sequence are printed by the computer and also punched in cards to form the data input deck for program SHRMOM.

### 3.3 Description of Program SHRMOM

The punched card output of CSUPLT is used as the total input data deck for SHRMOM. The input data consists of the column size, dimensionless ratios of  $H'$  and  $J'$ , geometric constants for node point numbering and the deflections at the node points of the plate. The program then computes and prints out the shears at the face of the column and one grid space from the face of the column; and moments in the x-direction, moments in the y-direction, twisting moments and principal moments in an area around the column bounded by the grid line 23 grid spaces from the center of the column.

## 4. RESULTS

### 4.1 Introductory Remarks

The results of the analyses of the mathematical model are presented herein for a series of column shapes and sizes. The response of the structure to a uniform load is presented in terms of the deflections along lines of symmetry and the moments and shears in the vicinity of the column.

Deflections are given for specimens with various column sizes and for test plates with various edge beam rigidities.

Moments along a line of symmetry are given for a typical specimen with a square column. Moments at the column face and one grid space from the column face are shown for the square columns.

Lines of contraflexure are shown and discussed for specimens with various column sizes. Position of these lines is discussed with respect to those in interior panels and clamped edge plates.

Shear force magnitude and distribution around the column is presented. Discussion on the accuracy and validity of the results is included.

Since the object of the study is the analysis of a particular real structure as shown in Fig. 1.1, the column sizes will be given in terms of inches and not as a fraction of the plate span length. The mathematical model Fig. 1.3 was analyzed for ten different column sizes. The four square columns analyzed included 16"x16", 12"x12",

8"x8" and 4"x4". Rectangular columns analyzed were (E-W dimension x N-S dimension) 16"x12", 16"x8", 16"x4", 12"x8", 12"x4" and 8"x4". Edge beam rigidities used were computed for the 6"x9" edge beam in Fig. 1.1 and are  $H' = 270.0$  and  $J' = 120.0$ . Poisson's ratio of the material was assumed equal to 0.15 throughout the study. \* Some special study was done in investigating the effect of edge beam rigidity on deflected shape and inflection point location.

Validity of the deflection solution was determined and is discussed in section 4.2.

#### 4.2 Deflections

Validity of the deflection solution for the mathematical model was determined by comparison with finite difference solutions of clamped edge plates obtained previously by Vanderbilt (17). Comparison was made for a square clamped edge plate with a point column in the center, and for a square clamped edge plate with a square column in the center. The side length of the square column was equal to one tenth the total plate span. Very large edge beam rigidities of  $J' = H' = 33,000.0$  were used to approximate a clamped edge on the mathematical model with a point column.  $J' = H' = 100,000.0$  were used for the mathematical model with a square column. Comparisons

---

\* A study of a test specimen having a 12"x12" column showed that for  $\mu = 0.00$  deflections were less than 1% larger than those obtained using  $\mu = 0.15$ .

of the results are shown in Fig. 4.1 and Fig. 4.2 where the two solutions show close agreement. Maximum difference between the two solutions is 4.5 percent for the point column solution and 6.75 percent for the square column solution. The grid spacing used in the clamped edge solution was three times as large as the grid used on the mathematical model. This grid size difference may be the cause of the clamped edge solution being consistently larger than the mathematical model solution.

The reinforced concrete test specimen (Fig. 1.1) was intended to simulate the state of stress around an interior column in a clamped edge plate (section 1.1). The flexural and torsional rigidities of the concrete test specimen were chosen to approximate the clamped edge boundary conditions. Deflection curves for the mathematical model with a 16" square column and various edge beam rigidities are shown in Fig. 4.3. The rigidities  $H' = 270.0$  and  $J' = 120.0$  are computed for the 6"x9" edge beam in the actual test specimen shown in Fig. 1.1. Notice the large rotation at the edge even for edge beam rigidities of  $H' = J' = 2000.0$ . Even very large edge beams do not produce the desired clamped edge condition. The dashed line is drawn through the inflection points and will be discussed in section 4.4.

Figures 4.4 and 4.5 are deflections along the N-S line of symmetry and the diagonal for the specimen with the four different square columns. The maximum deflection on the N-S line of

symmetry is approximately equal to the maximum deflection on the diagonal line of symmetry for each column size. Also the deflections decrease approximately in proportion to the increases in column size. Maximum deflection along these lines of symmetry occurs further from the column center as the column size is increased.

Deflections for the specimen for four different rectangular columns are shown in Figures 4.6 and 4.7. The rectangular columns all have an E-W dimension of 16" while the N-S dimension varies from 4" to 16". The two graphs show how the deflections change on both N-S and E-W lines of symmetry as the column size is changed in only the N-S dimension. Again, as with the square columns, the deflections decrease approximately in proportion to the increase in column size. The deflection decrease on the E-W line is about only half that on the N-S line for changes in N-S column dimensions.

### 4.3 Orthogonal Moments

A typical moment diagram for a midpanel line of symmetry is shown in Fig. 4.8. The plots of  $m_x$ ,  $m_y$  and  $m_{xy}$  are shown on an E-W line of symmetry for the test plate with a 16"x16" column.

The moments  $m_y$  at the north face of the column for the test structure with various square columns are shown in Fig. 4.9. Note that the maximum value is at the corner of the column and varies only about 17 percent over the size range of the square column. The moment distribution varies little with column size. The ratio of the

moment at the corner to the moment at the center of the column face varies from 1.6 for the 4"x4" column to 2.6 for the 16"x16" column.

The moments  $m_y$  at a distance of  $h = L/30$  from the north face of the four square center columns are shown in Fig. 4.10. The moments at  $h$  from the column corner are not nearly as large as those computed at the column corner except for the 4"x4" column.

#### 4.4 Lines of Contraflexure

The edge beams of the specimen under consideration (Fig. 1.1) were to have been rigid enough to effectively clamp the edge of the plate and eliminate any rotation or translation of the edge. Under these edge conditions the resulting lines of contraflexure would lie at  $L/6$  from the column face just as they do in an interior panel of a flat plate structure (section 1.1). Figure 4.11 shows the lines of contraflexure for principal moments for the specimens with square columns. The lines are nearly a constant  $L/4^*$  from the column face for all four columns. This is larger than the expected  $L/6$  and is a result of the edge beams not actually being rigid enough to consider the edges clamped.

The effect of edge beam rigidity on the position of the line of contraflexure is shown in Fig. 4.3 where the dashed line is drawn through the inflection points on the deflection curves. Even for very

\* Actual values range from  $L/4.27$  for the smallest column to  $L/4.00$  for the largest column.



rigid beams the inflection point lies at  $L/5.5$  from the column face. It should be noted that the  $L/6$  was determined previously (17) using a coarser grid than that used in this study.

The six Figs. 4.12 to 4.17 show the lines of contraflexure for the orthogonal moments  $m_x$  and  $m_y$  and the maximum principal moment  $m_{\max}$  for rectangular columns. In general  $m_{\max} = 0$  is  $L/4$  from both short and long column faces. When the ratio of the long to short face length is large such as 4 in the 16"x4" column the  $m_{\max} = 0$  line is  $L/4.4$  from the short column face and  $L/3.9$  from the long face.

#### 4.5 Shear at the Column

Shear forces at the corner point support, the column face, and at  $h = L/30$  from the column face were computed using the Newmark plate analog. These calculations were made for the test specimen of Fig. 1.1 with edge beam rigidities of  $J' = 120.0$  and  $H' = 270.0$ . Column size was the variable, with the ten different sizes indicated in section 4.1 being used.

A static equilibrium check of vertical forces acting on the northwest quarter of the plate was made. The object was to verify the shears calculated at the column face and at  $h$  from the column face for each column size. The three vertical forces on the quarter-plate are the load (downward), the shear at the corner point support (upward), and the shear at the column (upward).

The equilibrium check is shown in Table 4.1. Columns 2, 3, and 4 show the equilibrium check using the shears at the column face. Static equilibrium error is shown in column 4. Columns 5, 6, and 7 show the equilibrium check using the shears at  $h$  from the column face. Static equilibrium error is shown in column 7. Comparison of columns 4 and 7 indicates that the shears computed at  $h$  from the column face are far more accurate than those computed at the column face.

Shear force distribution at the face of the square columns is shown in Fig. 4.18. The computed maximum value of shear force, which occurs at the corner of the column, is very nearly the same for the three larger columns.

Shear force distribution at one grid space from the column face is shown in Fig. 4.19. The distribution remains nearly on the same line for all the square columns.

Using a much finer grid around the column Moe (8) and Ang (2) found the shears to be negative near the midpoint of the column face. Since similar results were not obtained during the present study one analysis of a specimen with an 8"x8" square column was made using a finer grid around the column. This particular column size was chosen because of the 17% error in equilibrium using shears at the column face (Table 4.1). A finer grid size with spacing  $h = L/60$  was used within a region bounded by a line at a distance of  $2L/15$  from the column, as shown in Fig. 4.20.

Deflections at points 1-25 were used as known boundary conditions. They were obtained either directly or by interpolation from the computer analysis with the coarser grid size  $h = L/30$ . Grid points shown in Fig. 4.20 with dark dots are those for which a deflection was known from using the coarser grid. Finite difference equations were written manually for points 26-88 and solved to obtain the deflections. Shears at the column face, at  $L/60$  from the column face and at  $L/30$  from the column face were computed and are shown in Fig. 4.21 along with similar results from the coarse grid analysis. A check of equilibrium of vertical forces showed that for the shears computed one grid space from the column, equilibrium was satisfied within 7%.

Shears near the column face midpoint are shown to be negative whereas the coarser grid did not indicate negative shear anywhere along the column face. The equilibrium check made using the shears computed at the column face satisfied equilibrium within 6% error.

Figure 4.22 shows the shear distribution on the column face for four rectangular columns all with a north face of 16". Shear distribution on the 16" face changes very little with the column size. Shear on the west face at the corner is nearly constant for all four column sizes.

Figure 4.23 shows the shear distribution at  $h = L/30$  from the faces of the four rectangular columns with 16" north faces. The shear distribution changes little on either face.

## 5. SUMMARY, DISCUSSION AND CONCLUSIONS

### 5.1 Summary

The results of the analyses of an elastic mathematical model of a new type of shear test specimen (Fig. 1.3) are presented.

Emphasis is on the structural behavior around the center support of the test specimen.

The analyses were performed using the calculus of finite differences and Newmark's plate analog. The development of the operators is given in Chapter 2 and the computer programs used in generating and solving the finite-difference simultaneous equations are described in Chapter 3 and the Appendices.

The results of the analyses are given in Chapter 4 in terms of deflections, shears, moments, and positions of lines of contraflexure near the column for test specimens with ten various column sizes.

### 5.2 Discussion and Conclusions

The reinforced concrete test specimen used in another phase of this study and analyzed herein is shown in Fig. 1.1. Based on studies of elastic plates this specimen was designed to simulate the structural behavior in the vicinity of a column supporting an interior panel of a continuous multi-panel flat plate structure. The mathematical elastic model shown in Fig. 1.3 models the reinforced concrete specimen of Fig. 1.1.

As shown in Fig. 4.3 and 4.11 the new test specimen does not model the elastic behavior of an interior panel as closely as had been desired. The lines of contraflexure for the new test specimen lie at about  $L/4$  from the column face rather than the  $L/6$  reported previously (10). The dashed line drawn through the inflection points in Fig. 4.3 shows that extremely large values of beam rigidities ( $H'$ ,  $J'$ ) are necessary to simulate the clamped edge condition. It may be concluded that the test specimen more closely simulates the structural behavior around an interior column supporting four corner panels (Fig. 5.1) than the typical interior column desired.

As is shown in Fig. 4.18 the shears computed along the column face are concentrated at the corner of the column. The changes in the slope of the deflection surface at the corner of the column are too large and abrupt to permit an accurate approximation using the finite difference method. Therefore errors are encountered in computing shears at the face of the column as is shown in Table 4.1.

The distribution shown in Fig. 4.18 is for the elastic structure and would change as plastic deformation occurs at the highly stressed corners.

The shear in Fig. 4.19 at one grid space from the column satisfied equilibrium within 0.61% for all column sizes which indicates that the finite difference method accurately describes the stress near but not at the column corner.

The refined grid study described in section 4.5 shows that the grid size used in this study was too coarse to indicate negative shear near the midpoint of the face as was reported by previous investigators (2, 8).

The test specimen does closely simulate the state of stress around an interior column in a continuous flat plate structure. Experimental testing of the model under uniform loads should provide useful data to contribute to the understanding of reinforced concrete flat plates.

## BIBLIOGRAPHY

1. Anderson, Decima M., Computer Programming FORTRAN IV. New York: Appleton-Centry-Crofts, 1966.
2. Ang, A.H.S., and Siess, C.P., "Bond in Flat Slabs," American Concrete Institute, Journal, 57: 1512-21, Concrete Briefs, May 1961.
3. Grow, J.B., and Vanderbilt, M.D., "A Study of the Shear Strength of Lightweight Prestressed Concrete Flat Plates," Colorado State University, Department of Civil Engineering, Structural Research Report No. 2, Fort Collins, December 1966, 48 p.
4. Hanson, Norman W., and Hanson, John M., "Shear and Moment Transfer Between Concrete Slabs and Columns," Portland Cement Association Research and Development Laboratories, Development Department, Bulletin D129, Skokie, Illinois, January 1968, 16 p.
5. Ivy, Charles Benjamin, "The Diagonal Tension Resistance of Structural Lightweight Concrete Slabs," Texas A&M, College Station, January 1966, (Ph.D. Dissertation).
6. Kinnunen, S., and Nylander, H., "Punching of Concrete Slabs Without Shear Reinforcement," Transactions, Swedish Royal Institute of Technology, Stockholm, No. 158, 1960, 112 p.
7. McCracken, Daniel D., A Guide to FORTRAN IV Programming. New York: John Wiley and Sons, Inc., 1966.
8. Moe, Johannes, "Shearing Strength of Reinforced Concrete Slabs and Footings Under Concentrated Loads," Portland Cement Association Research and Development Laboratories, Development Department, Bulletin D47, Skokie, Illinois, April 1961, 135 p.
9. Mowrer, R.D., and Vanderbilt, M.D., "A Study of the Shear Strength of Lightweight Reinforced Concrete Flat Plates," Colorado State University Department of Civil Engineering, Structural Research Report No. 1, Fort Collins, August 1966, 77 p.

10. Mowrer, R.D., and Vanderbilt, M.D., "Shear Strength of Lightweight Aggregate Reinforced Concrete Flat Plates," American Concrete Institute, Journal, 64: 722-29, November 1967.
11. Prescott, W.S.; Ang, A.; and Siess, C.P., "Analysis of Clamped Square Plates Containing Opening with Stiffened Edges," Illinois University Department of Civil Engineering, Structural Research Series No. 229, Urbana, November 1961, 202 p.
12. Salvadori, Mario G., and Baron, Melvin L., Numerical Methods in Engineering. Englewood Cliffs, N.J.: Prentice-Hall, Inc., 1961.
13. Spillers, W.R., "Techniques for Analysis of Large Structures," ASCE Structural Division, Journal, Vol. 94 (ST11): 2521-34, November 1968.
14. Timoshenko, S., and Woinowsky-Krieger, S., Theory of Plates and Shells. New York: McGraw-Hill Book Company, 1959.
15. Timoshenko, S., and Young, D.H., Elements of Strength of Materials. Princeton, N.J.: D. Van Nostrand Co., Inc., 1962.
16. Vanderbilt, M.D.; Sozen, M.A.; and Siess, C.P., "Deflection of Reinforced Concrete Floor Slabs," Illinois University Department of Civil Engineering, Structural Research Series No. 263, Urbana, April 1963, 287 p.
17. Vanderbilt, M.D., Unpublished report, Department of Civil Engineering, Colorado State University.
18. Wylie, Jr., C.R., Advanced Engineering Mathematics. New York: McGraw-Hill Book Company, 1966.

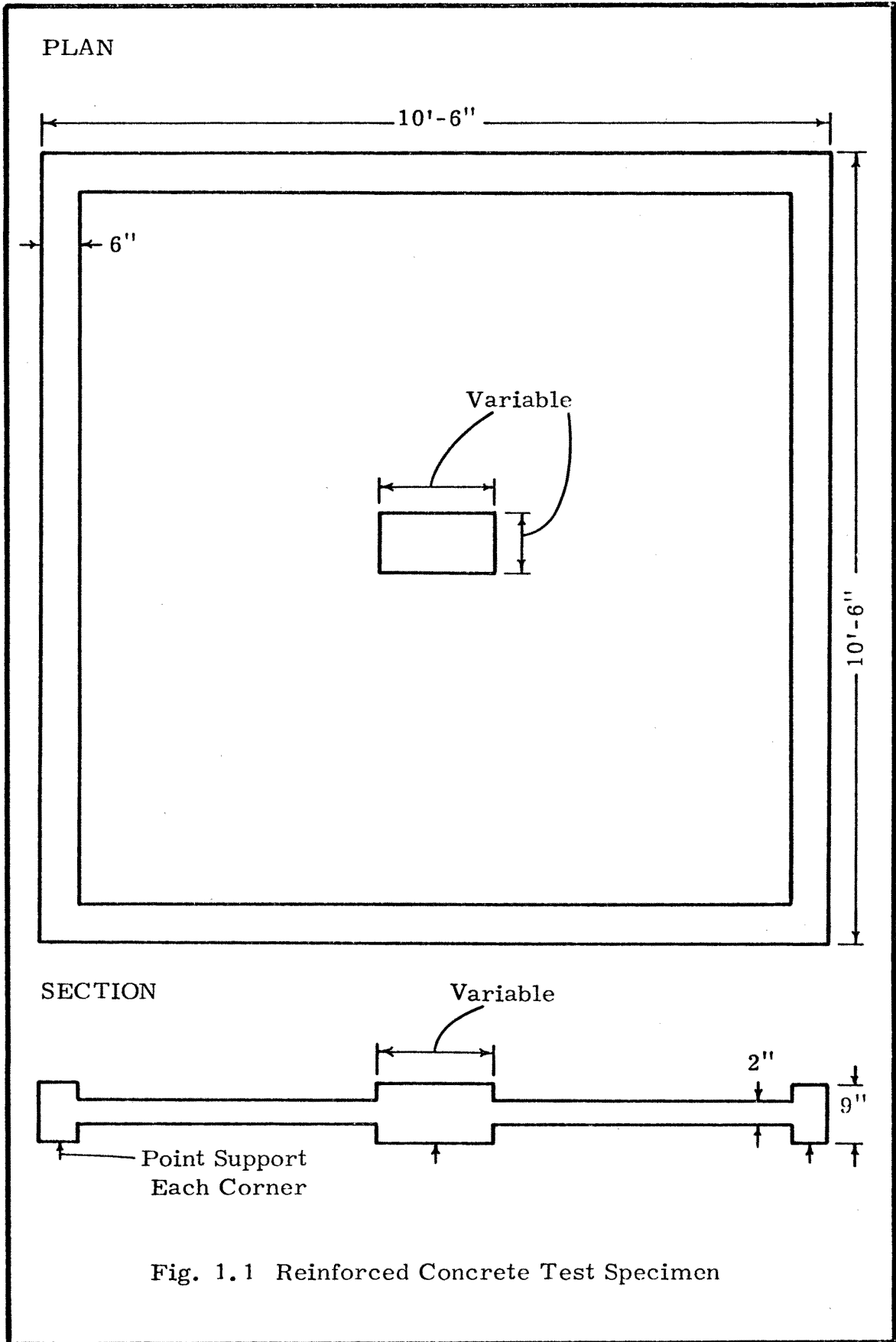


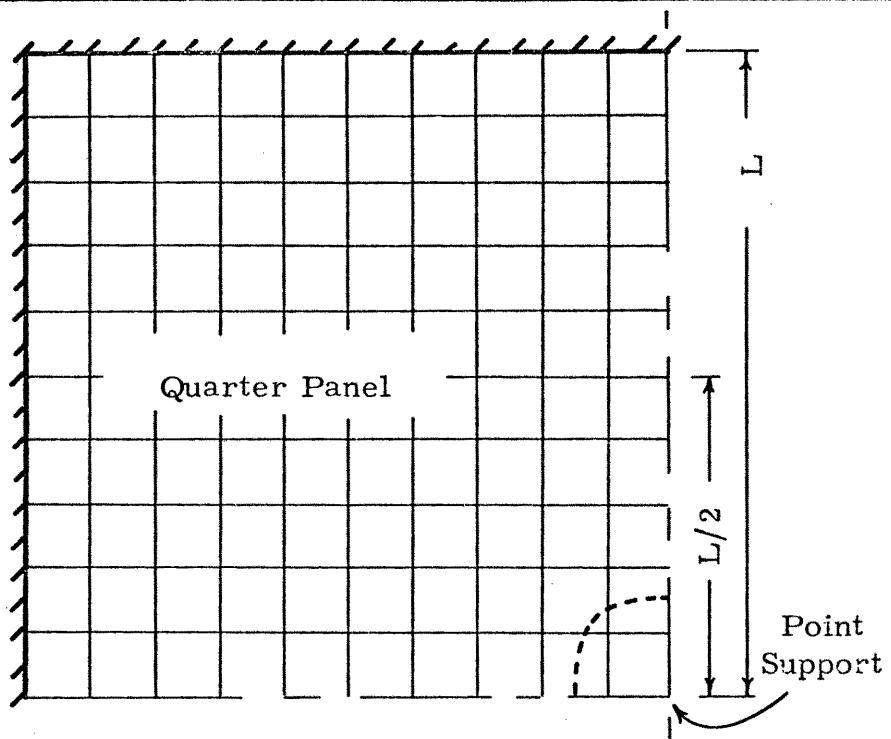
(1) Column Size (inches)	(2) Load Down Outside of Column $qL^2$	(3) Beam Shear + Shear at Column Face $qL^2$	(4) Equilibrium Error for (3) $\frac{(3)-(2)}{(2)}$	(5) Load Down Outside of 2" from Column $qL^2$	(6) Beam Shear + Shear at 2" from Column Face $qL^2$	(7) Equilibrium Error for (6) $\frac{(6)-(5)}{(5)}$
4x4	.9989	1.1055	10.67%	.9956	.9928	-.28%
8x4	.9978	1.1524	15.49%	.9933	.9900	-.36%
8x8	.9956	1.1667	17.19%	.9900	.9862	-.39%
12x4	.9967	1.1454	14.92%	.9911	.9873	-.38%
12x8	.9933	1.1477	15.54%	.9867	.9823	-.45%
12x12	.9900	1.1246	13.60%	.9822	.9774	-.49%
16x4	.9956	1.1127	11.76%	.9889	.9845	-.44%
16x8	.9911	1.1097	11.97%	.9833	.9785	-.49%
16x12	.9867	1.0843	9.89%	.9778	.9724	-.55%
16x16	.9822	1.0444	6.33%	.9772	.9663	-.61%

12.74% avg

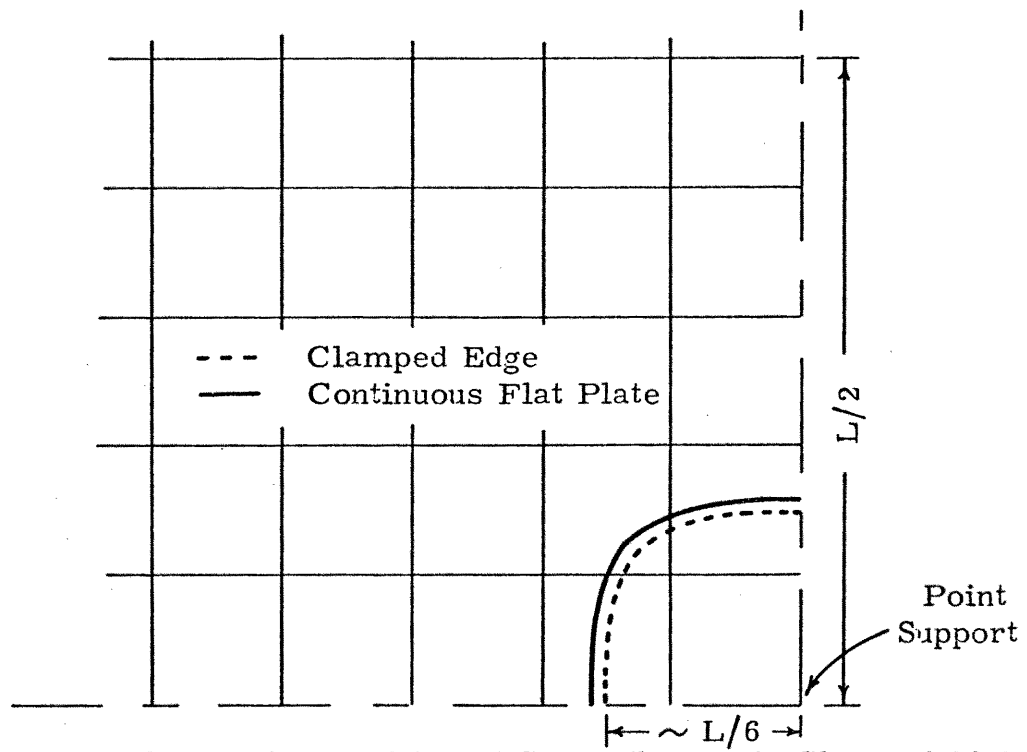
-.44% avg

Table 4.1 Equilibrium Check of Shear Forces





a. Clamped Edge Plate Showing Line of Contraflexure



b. Comparison of Line of Contraflexure in Clamped Plate With Line for Continuous Interior Panel

Fig. 1.2

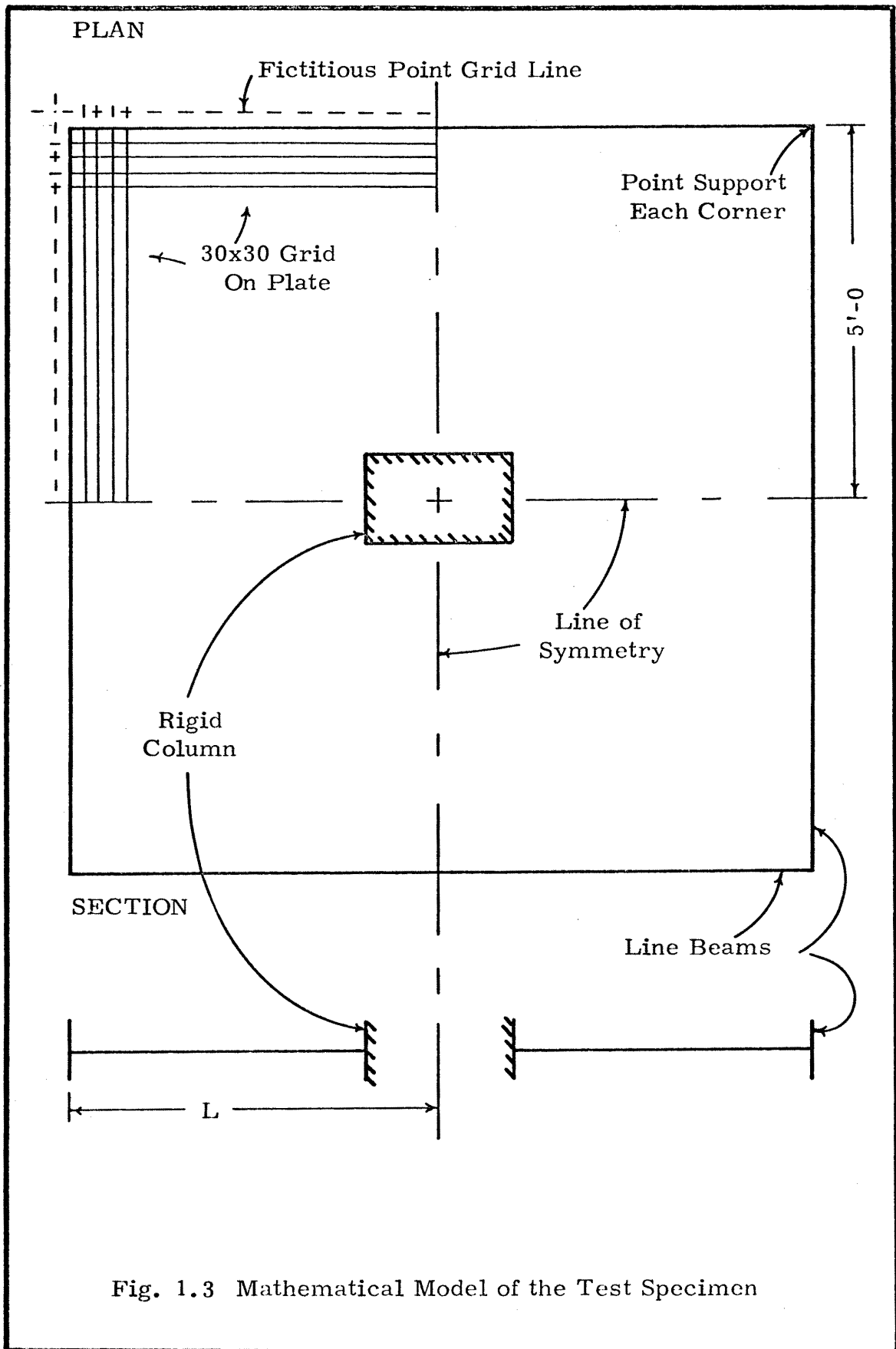


Fig. 1.3 Mathematical Model of the Test Specimen

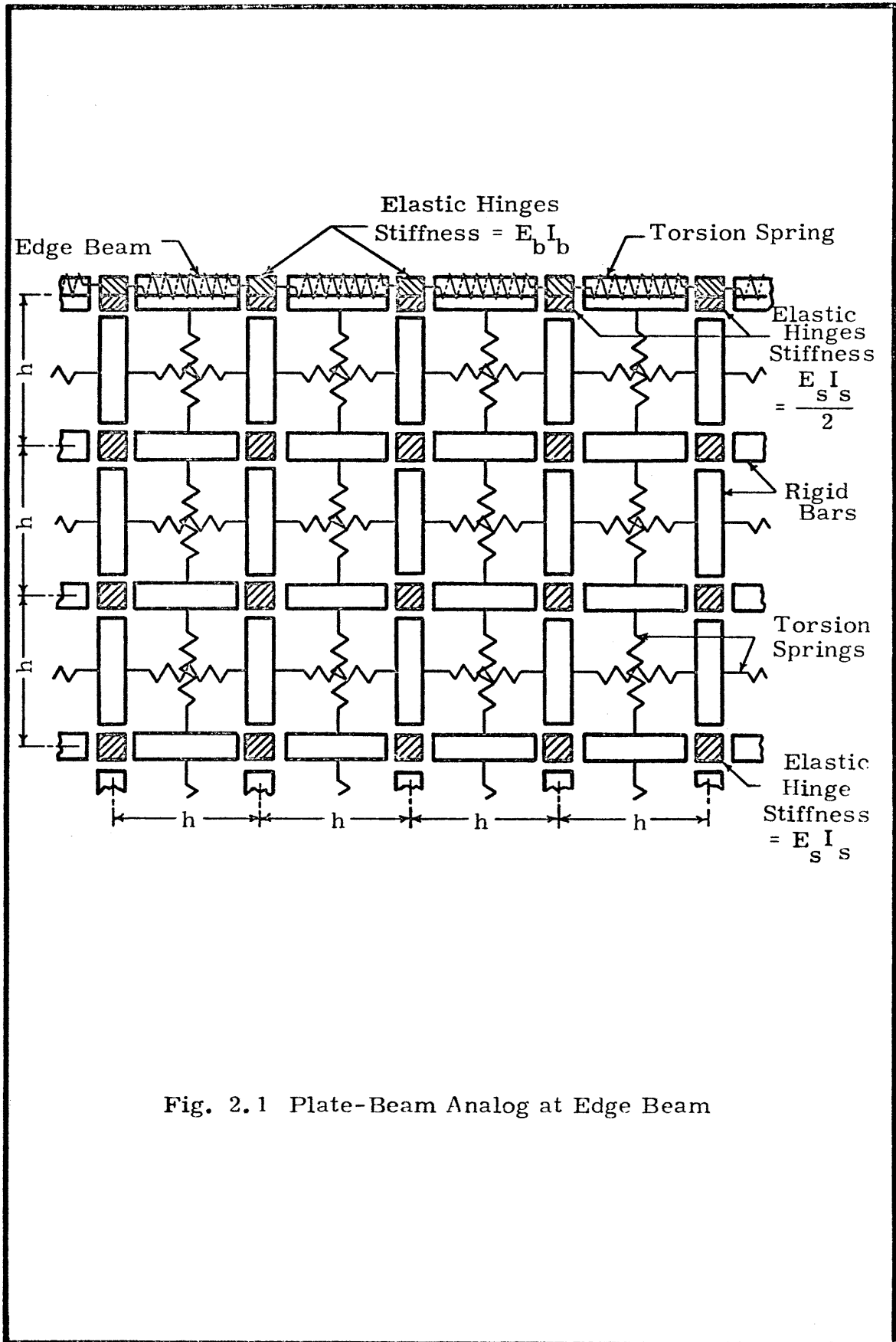


Fig. 2.1 Plate-Beam Analog at Edge Beam

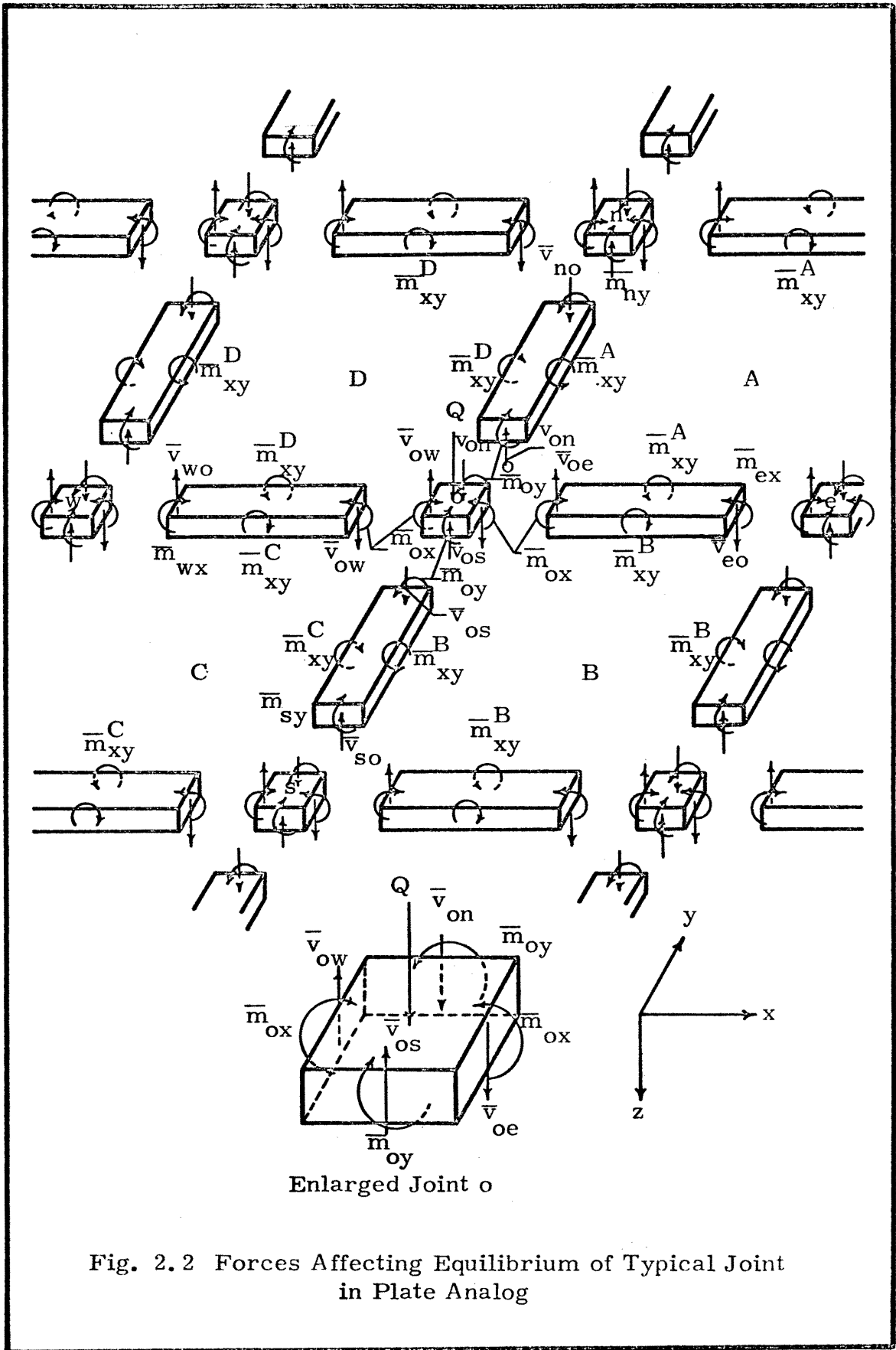


Fig. 2.2 Forces Affecting Equilibrium of Typical Joint in Plate Analog

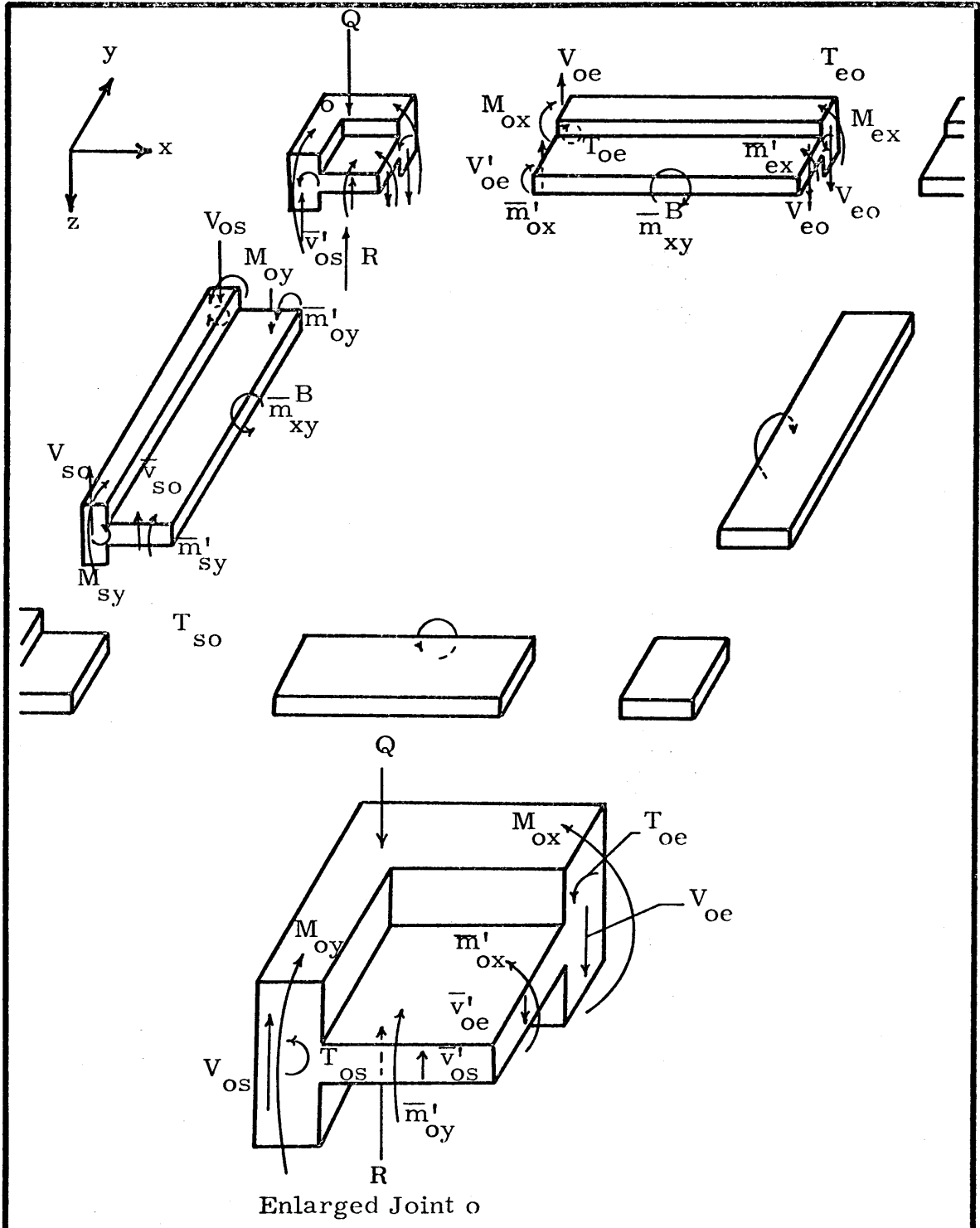


Fig. 2.3 Forces Affecting Equilibrium at Edge Beam Corner Joint in Plate-Beam Analog

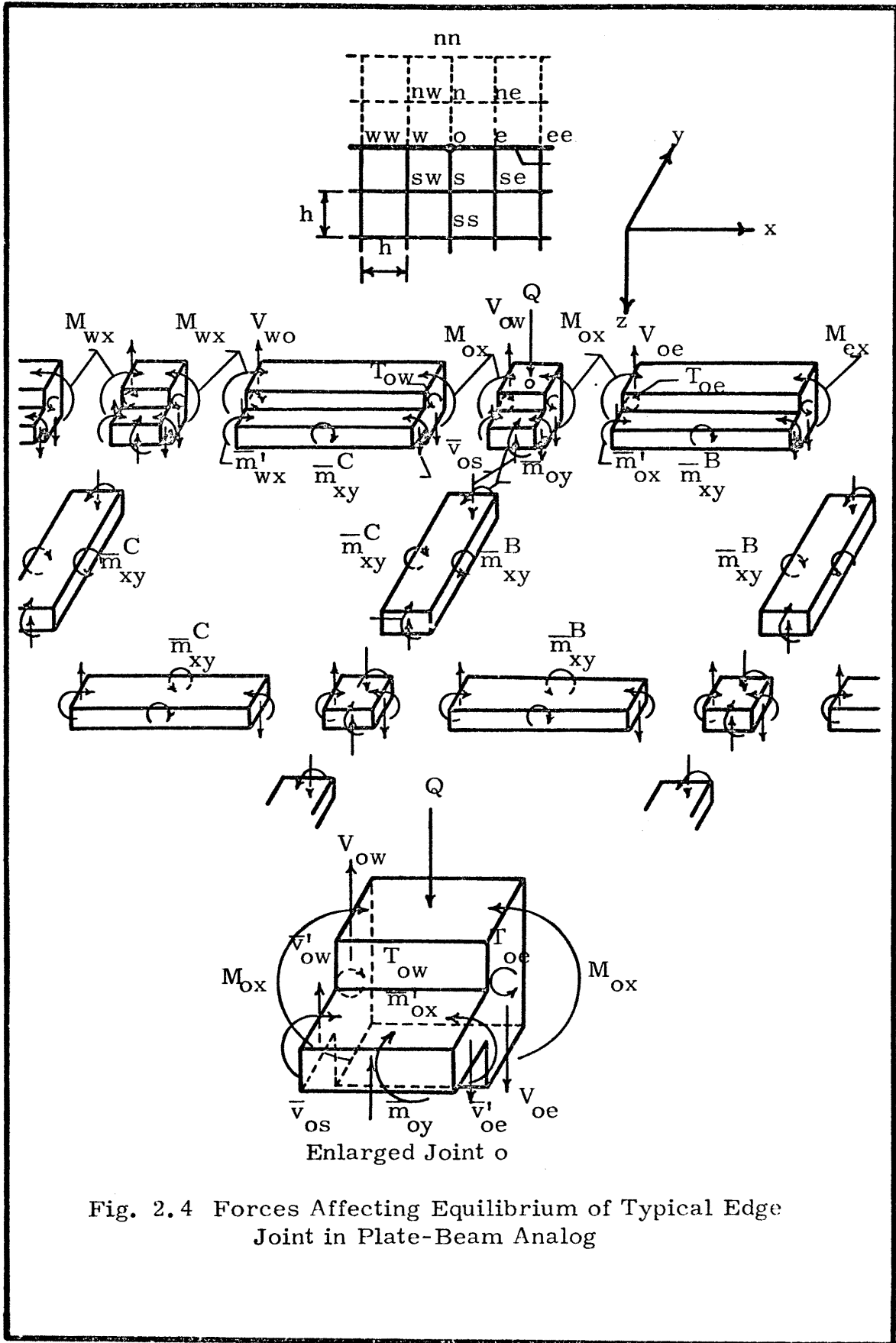


Fig. 2.4 Forces Affecting Equilibrium of Typical Edge Joint in Plate-Beam Analog



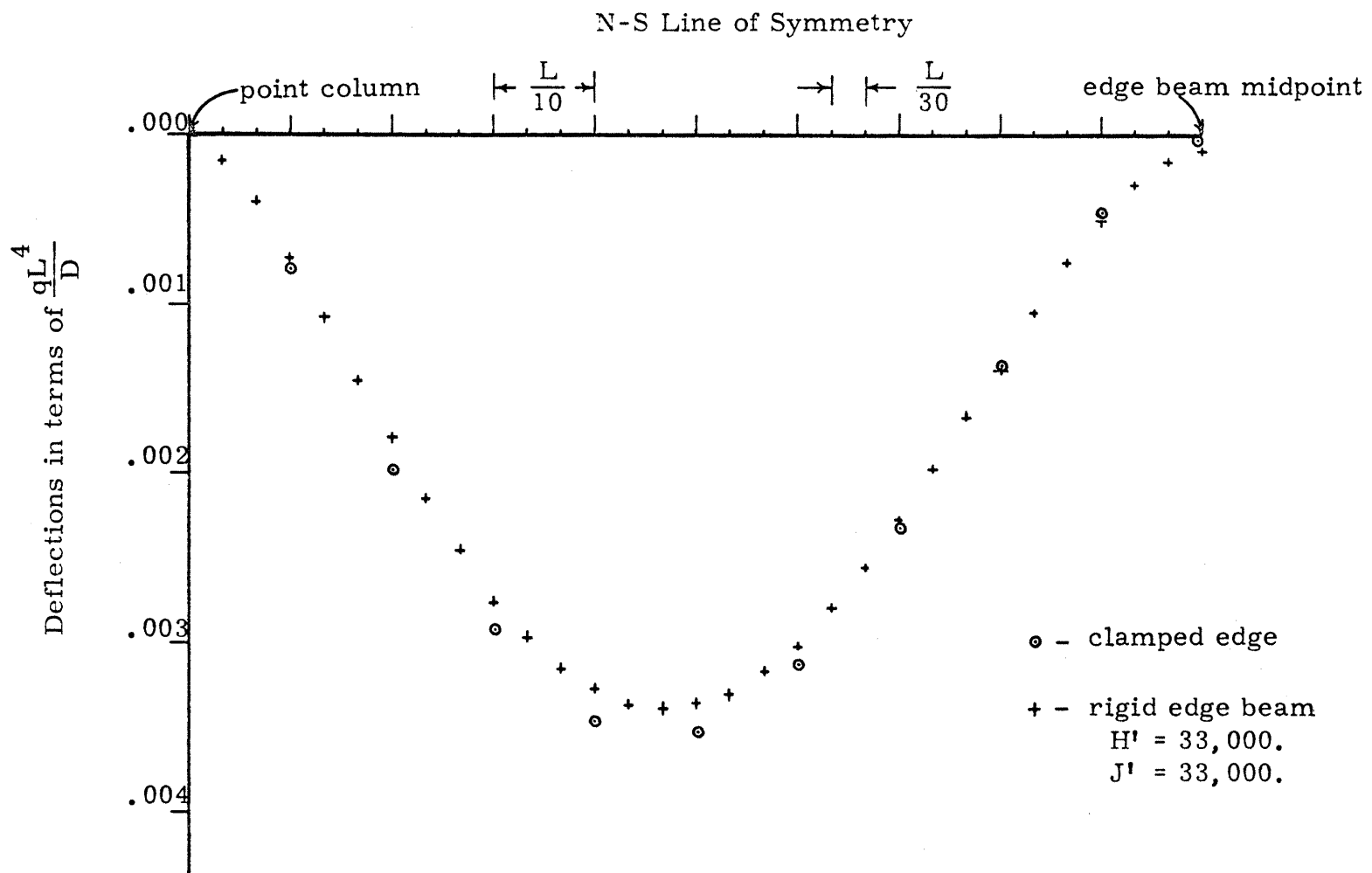


Fig. 4.1 Comparison of Deflections on N-S Line of Symmetry For a Specimen with a Point Column

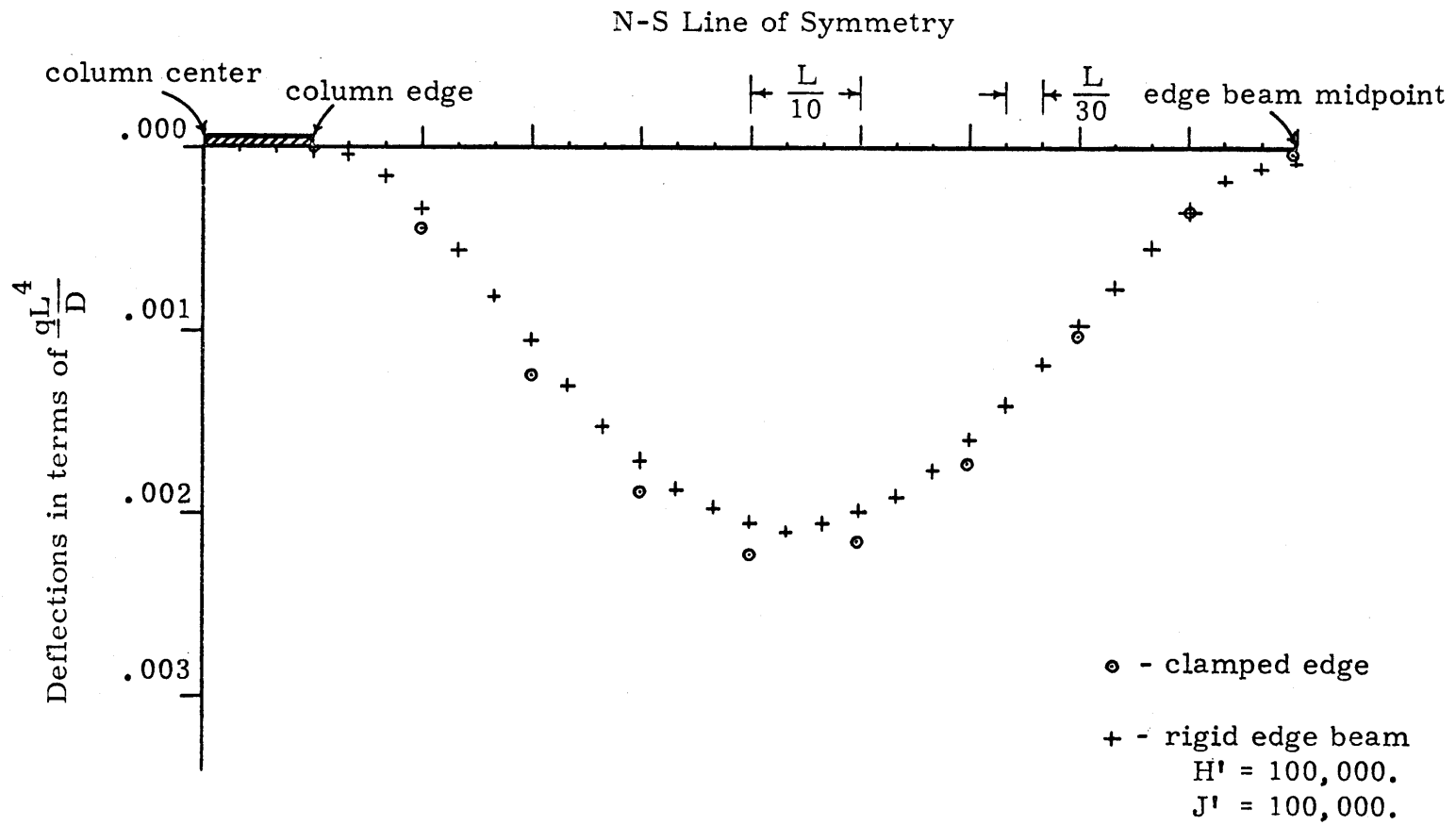
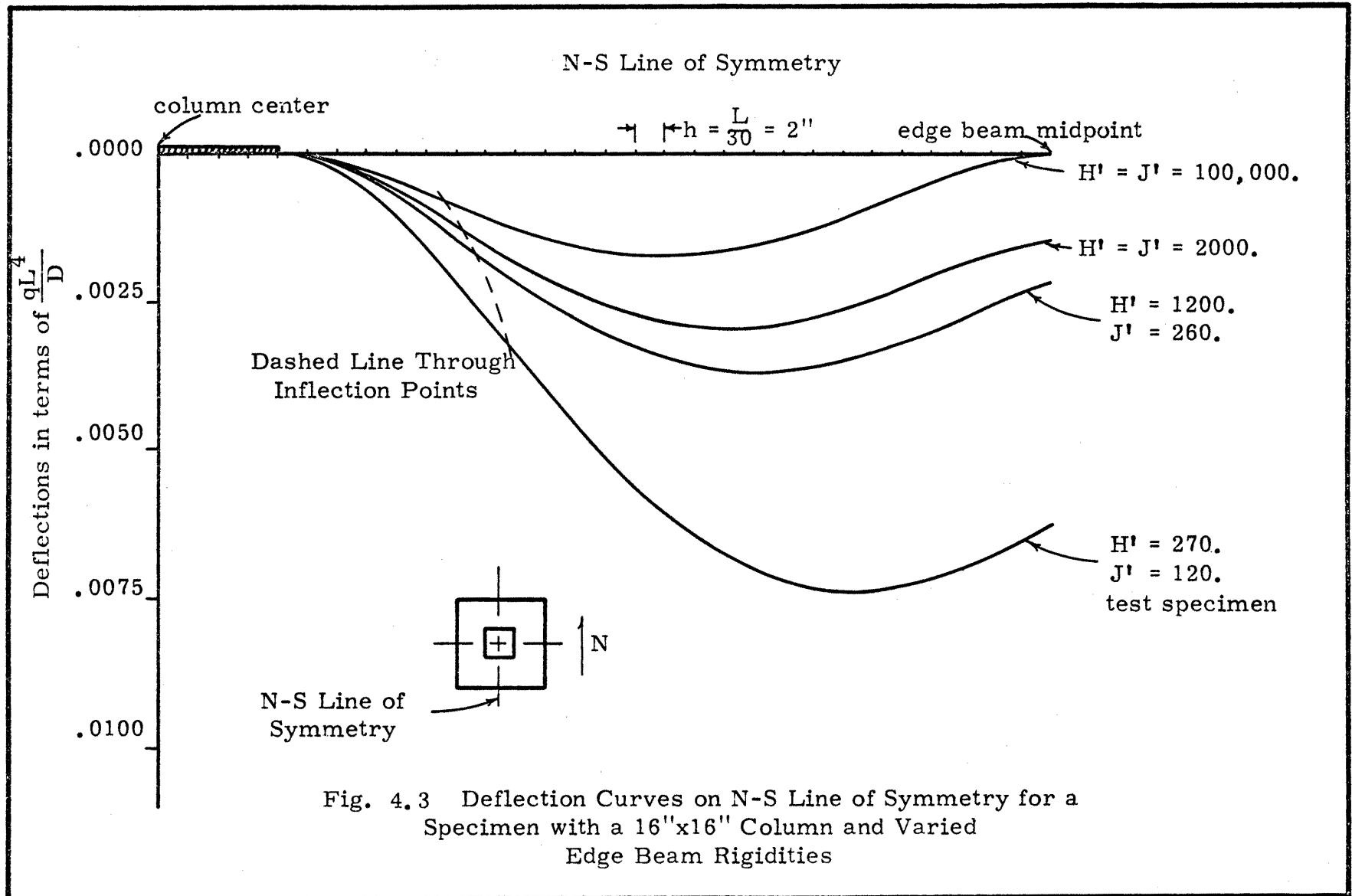
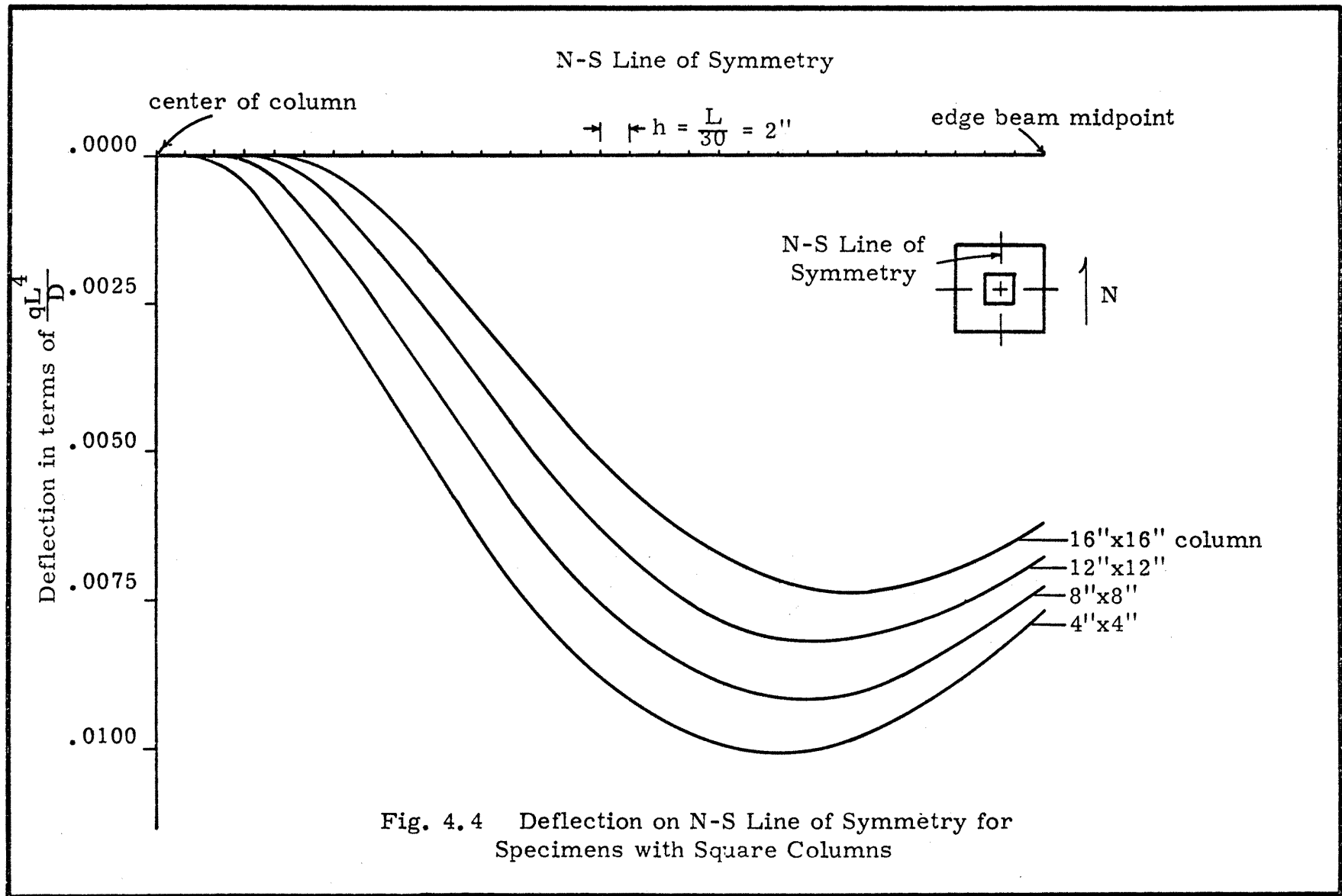
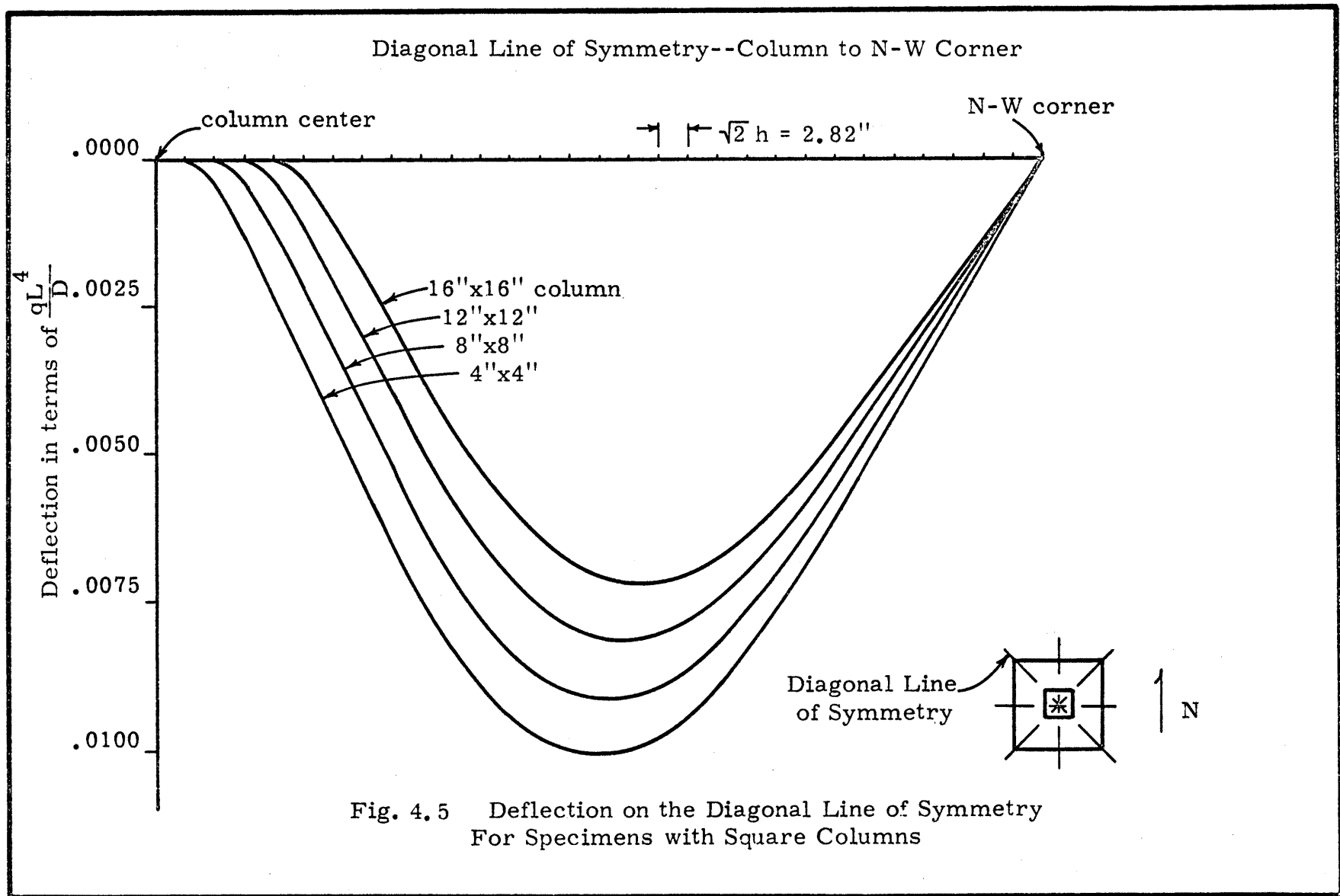


Fig. 4.2 Comparison of Deflections on N-S Line of Symmetry  
For a Specimen with a 12"x12" Square Column







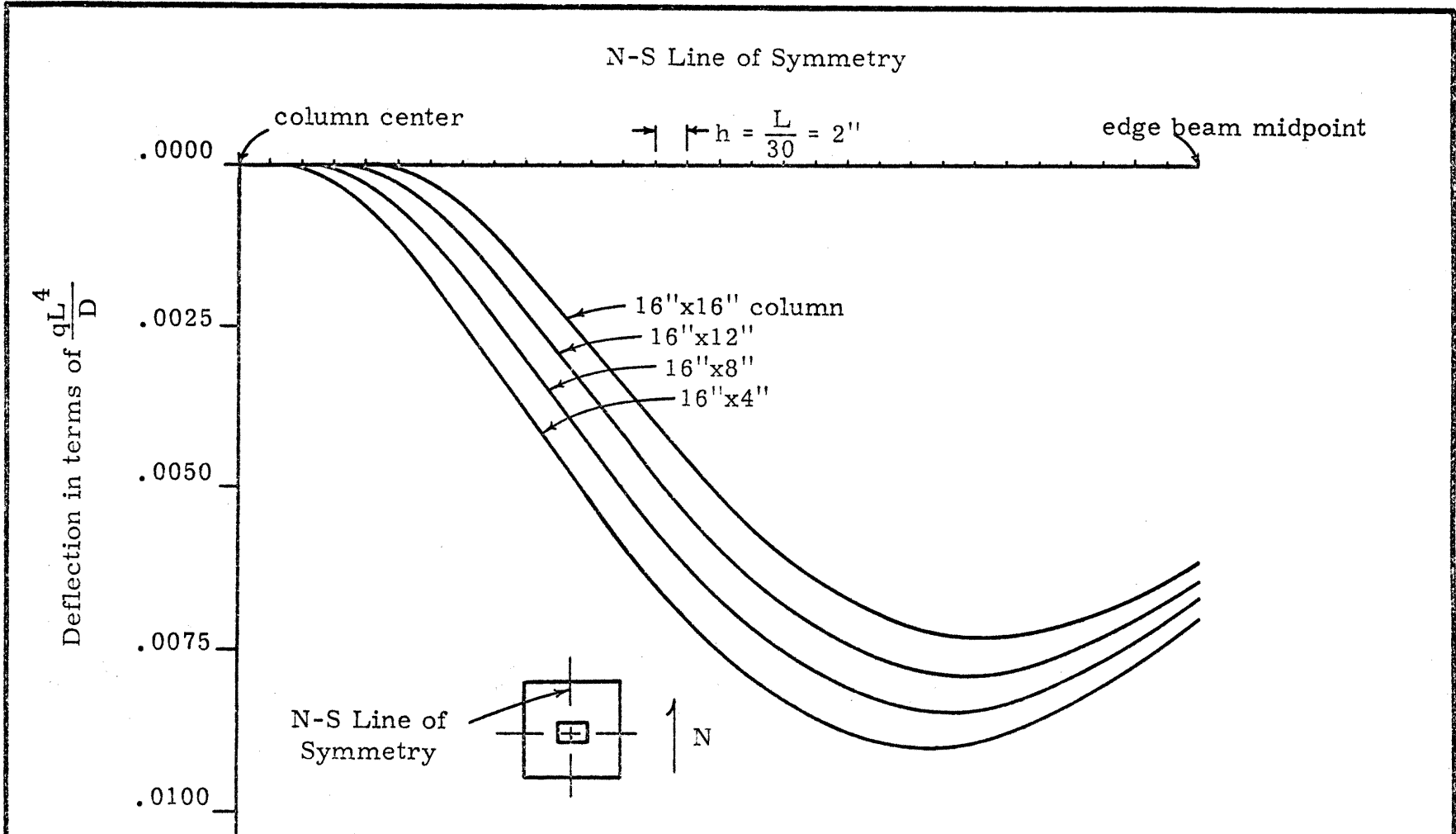
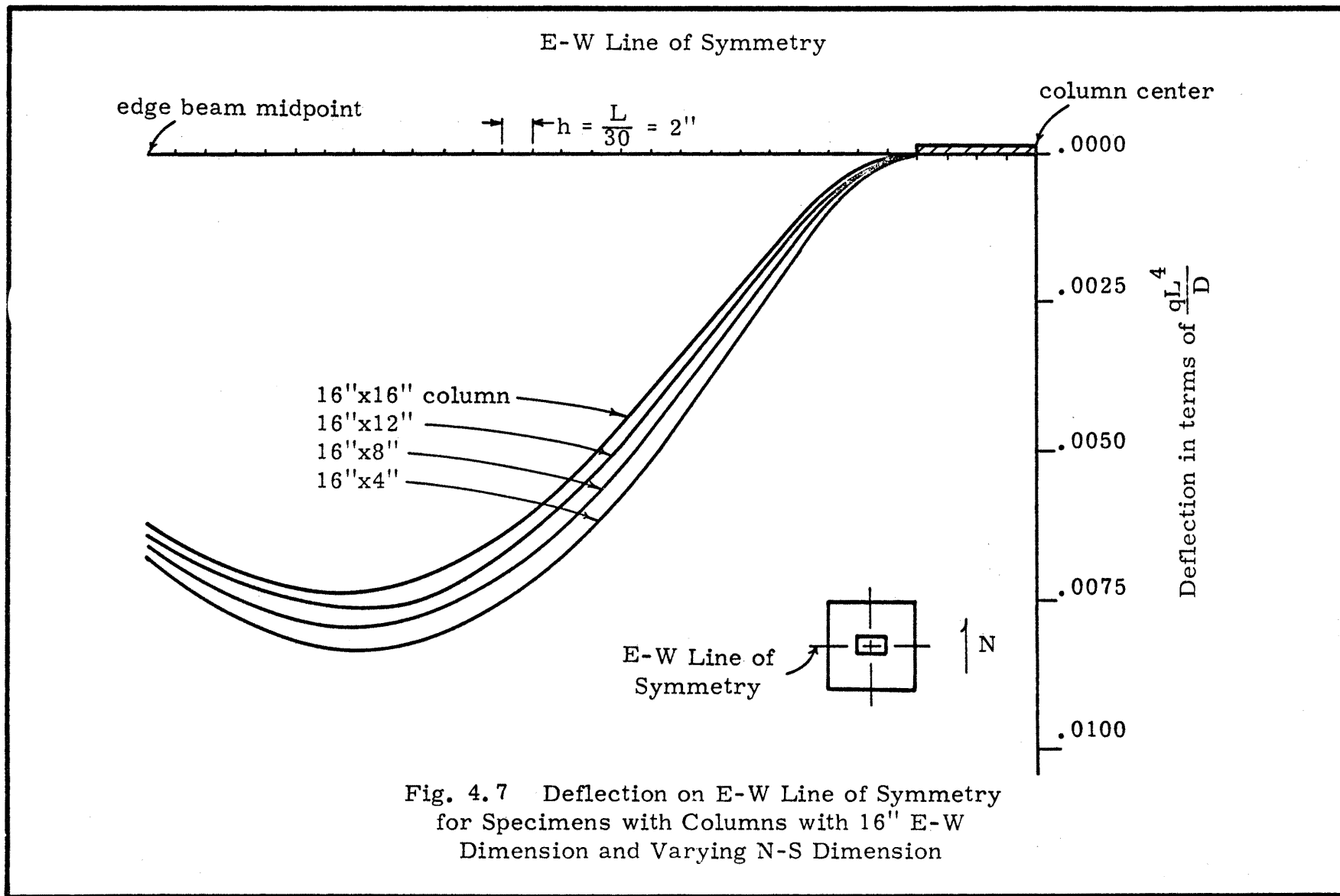


Fig. 4.6 Deflection on N-S Line of Symmetry for Specimens With Columns with 16'' E-W Dimension and Varying N-S Dimension



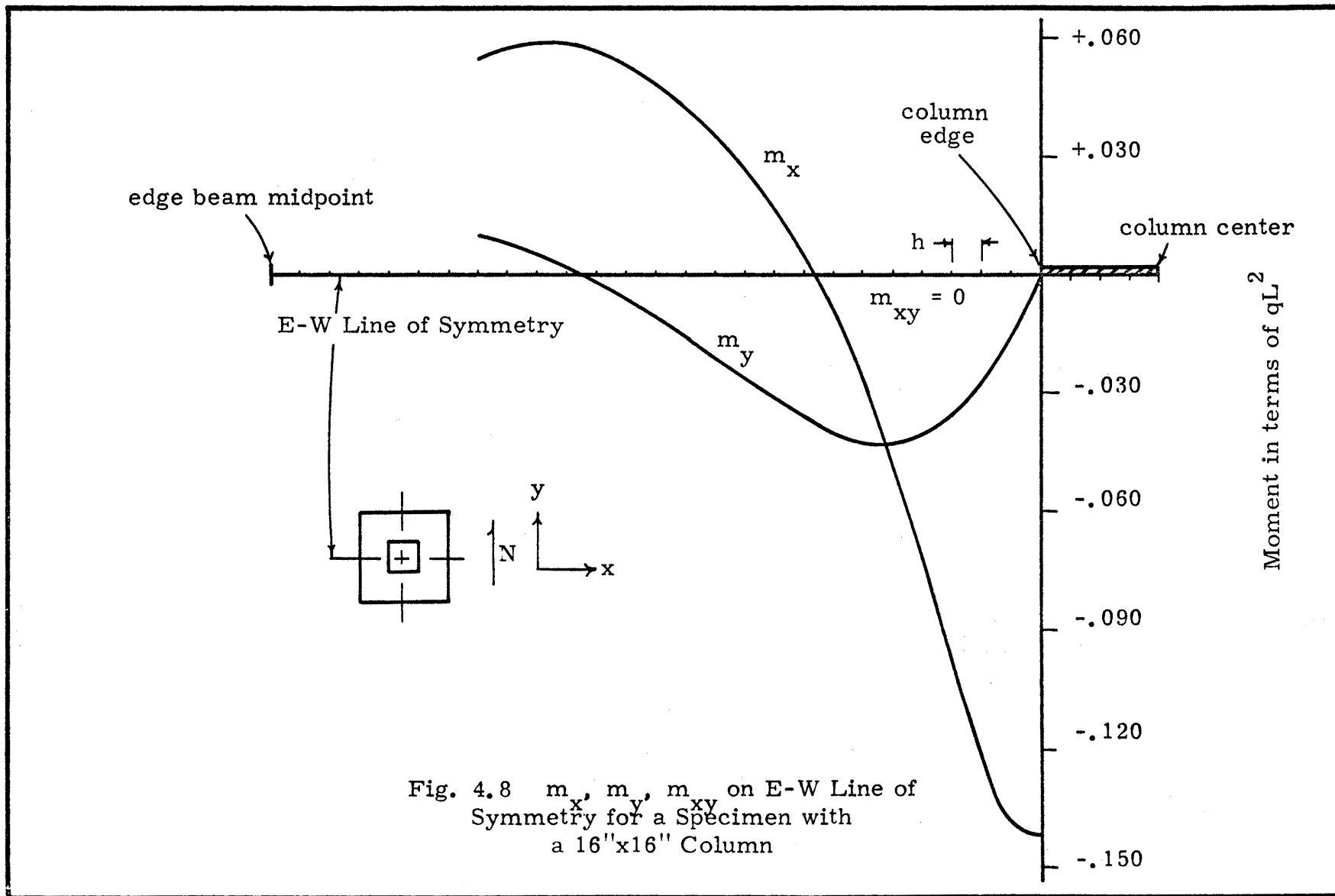


Fig. 4.8  $m_x$ ,  $m_y$ ,  $m_{xy}$  on E-W Line of Symmetry for a Specimen with a 16''x16'' Column



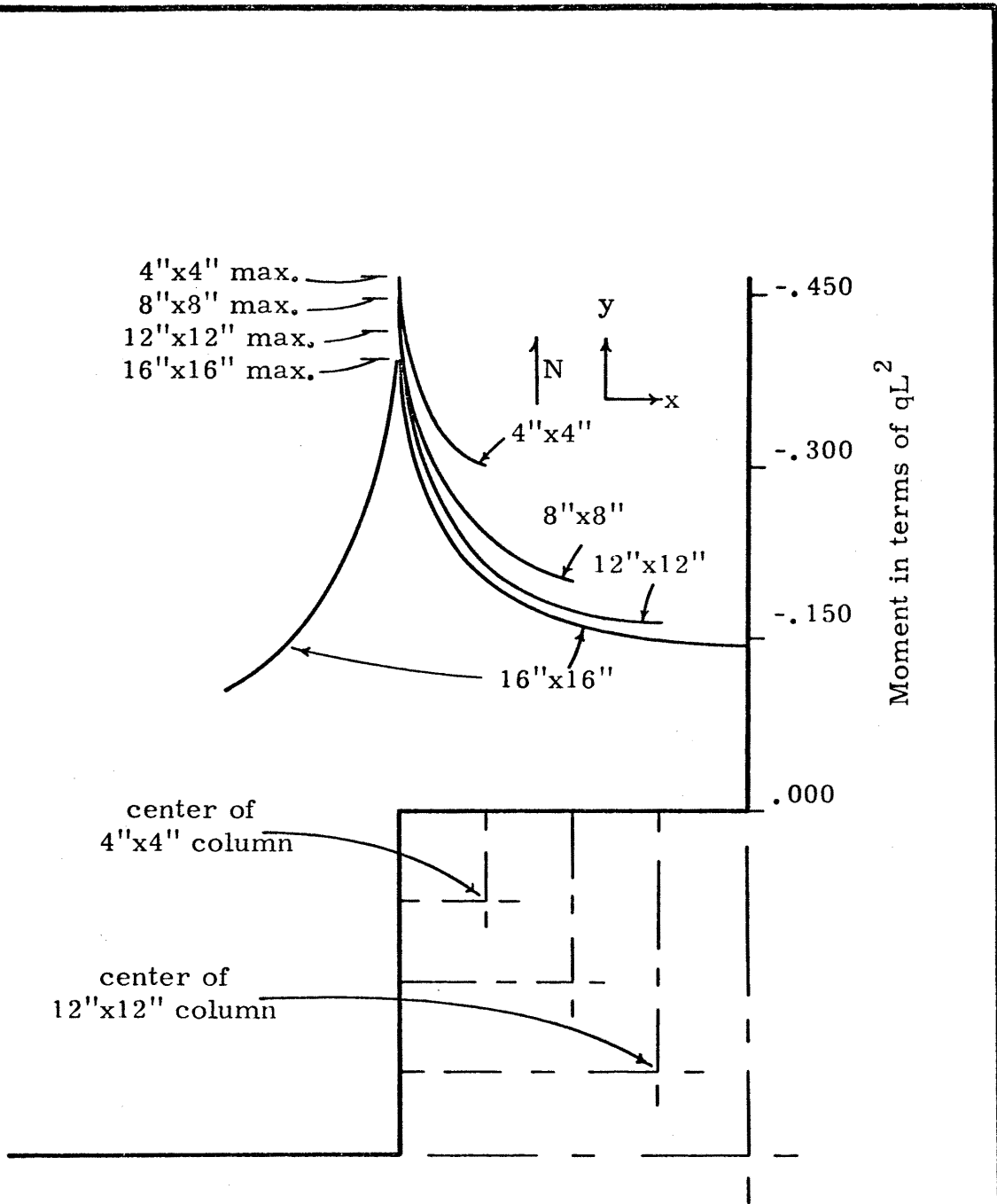


Fig. 4.9 Moment  $m_y$  at the Face of the Square Columns in the Test Specimens

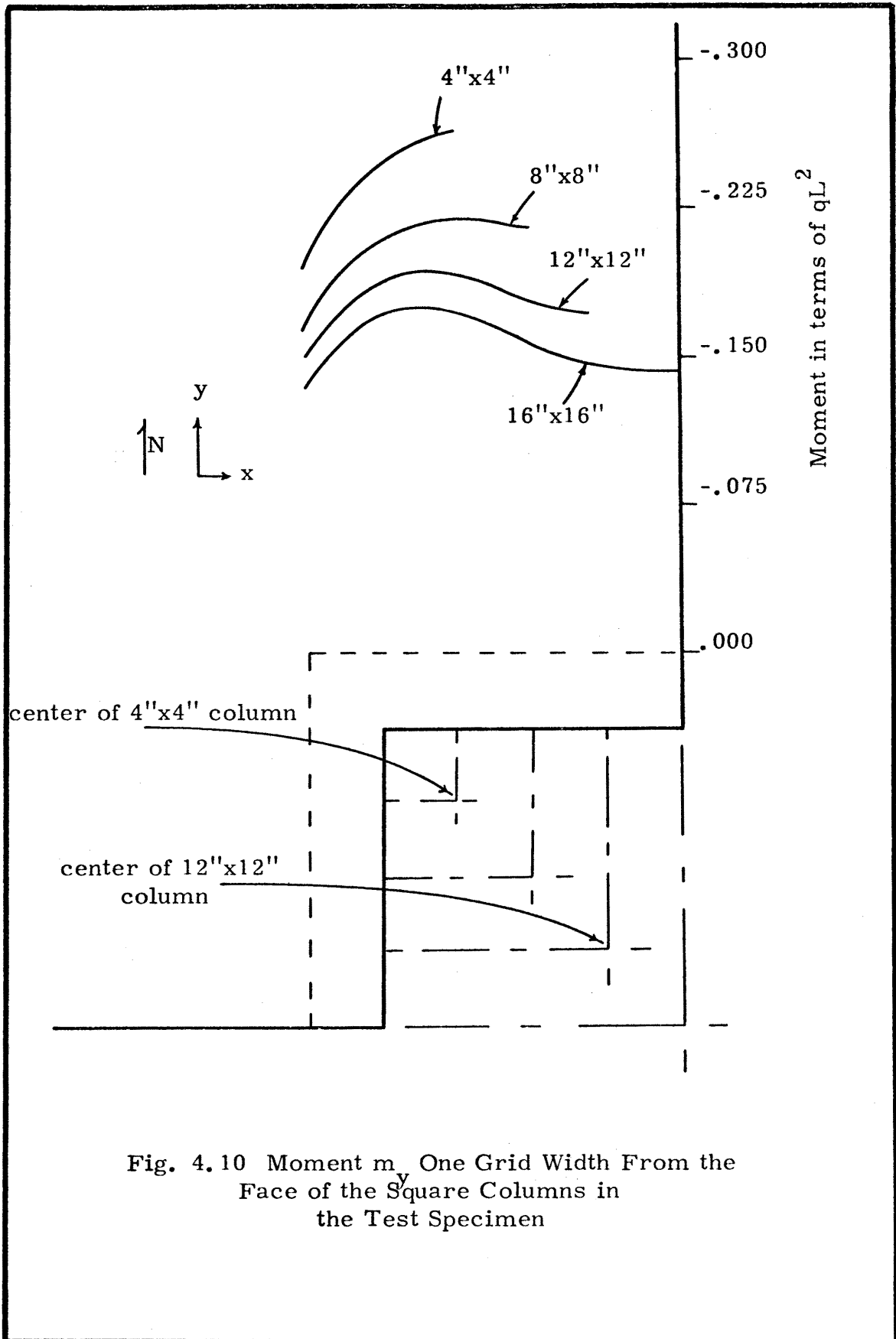


Fig. 4.10 Moment  $m_y$  One Grid Width From the Face of the Square Columns in the Test Specimen

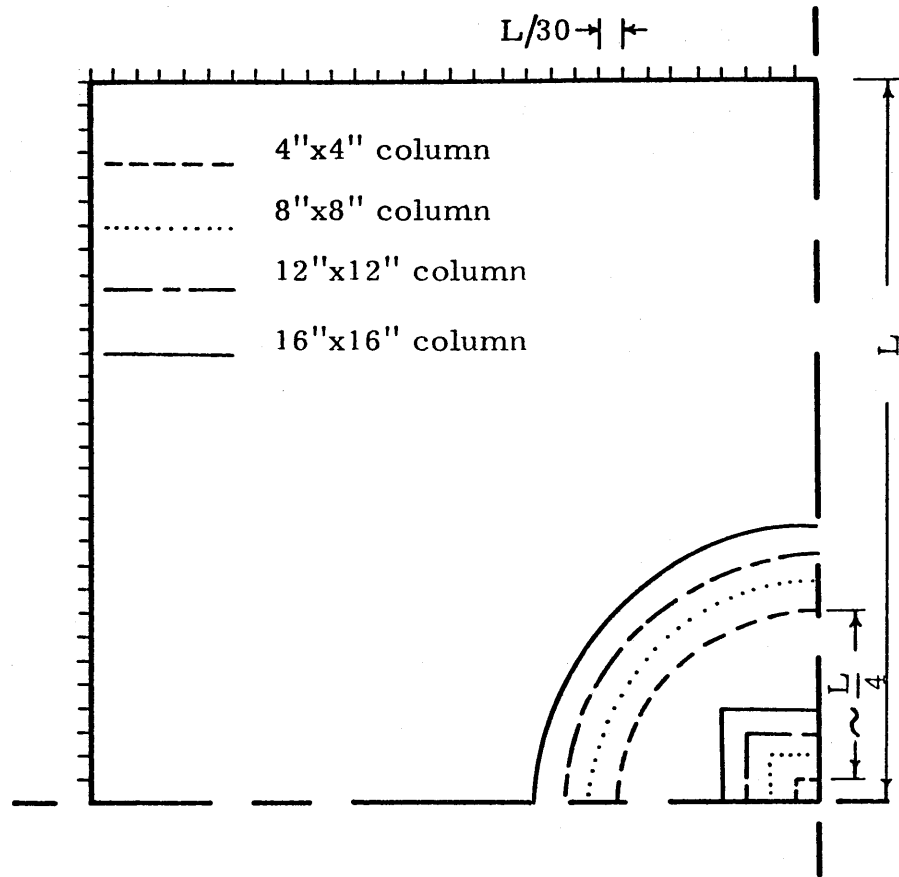


Fig. 4.11 Lines of Contraflexure for Principal Moments about Square Columns in the Specimen

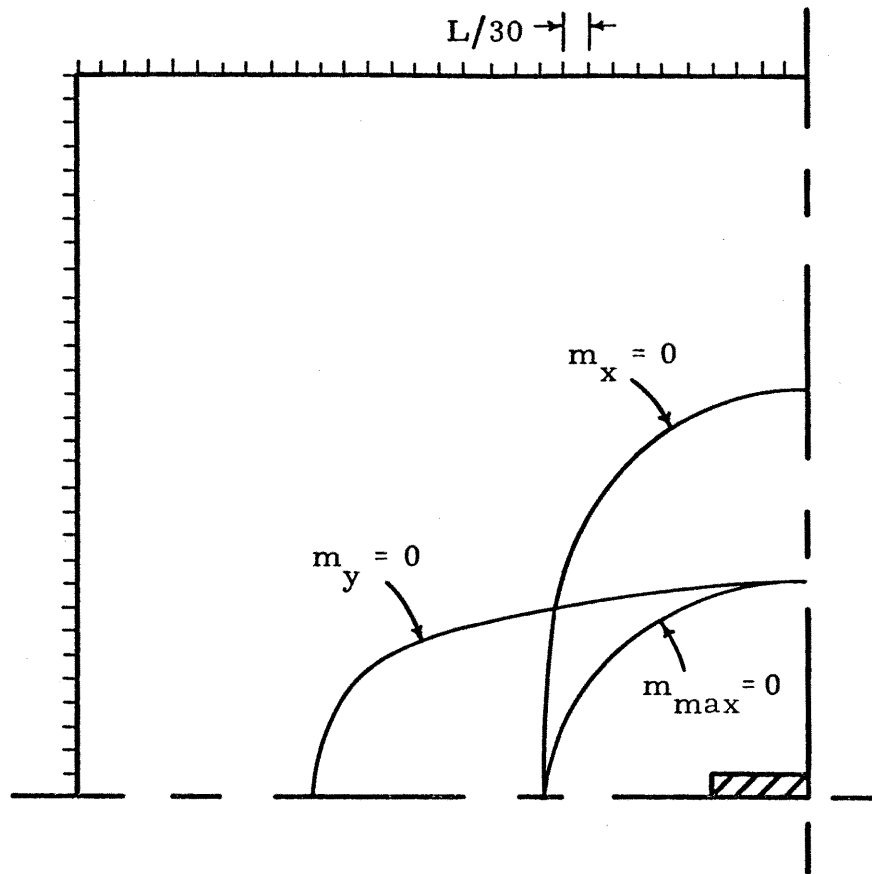


Fig. 4.12 Lines of Contraflexure  
Around a 16''x4'' Column  
in the Specimen

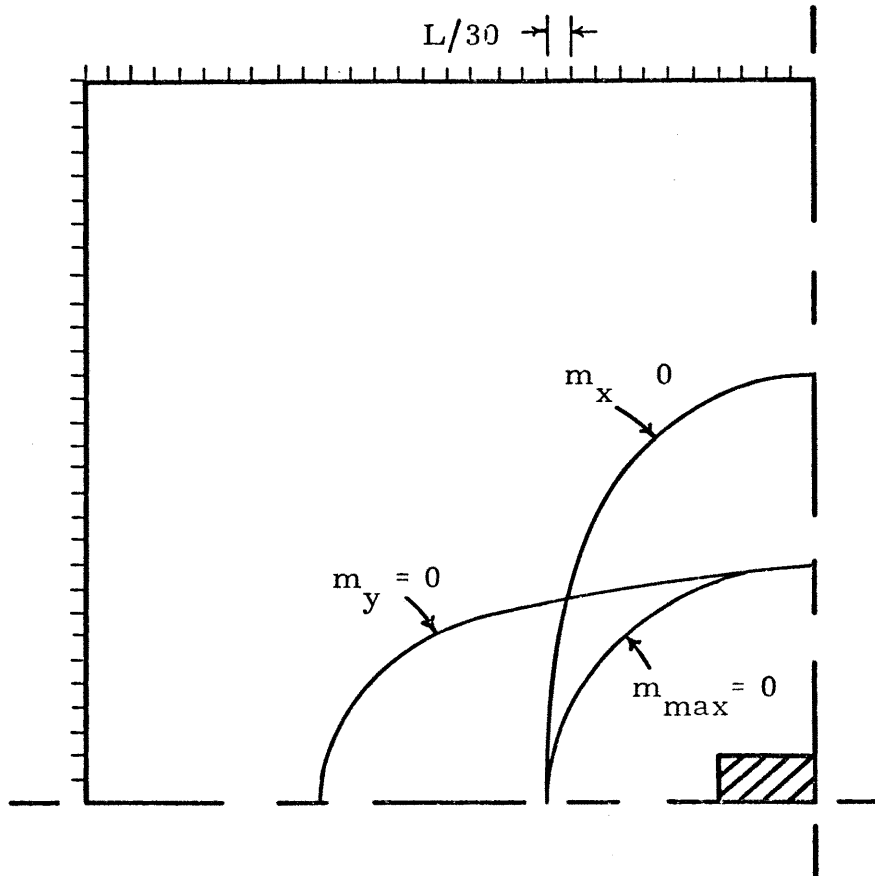


Fig. 4.13 Lines of Contraflexure Around  
a 16"x8" Column  
in the Specimen

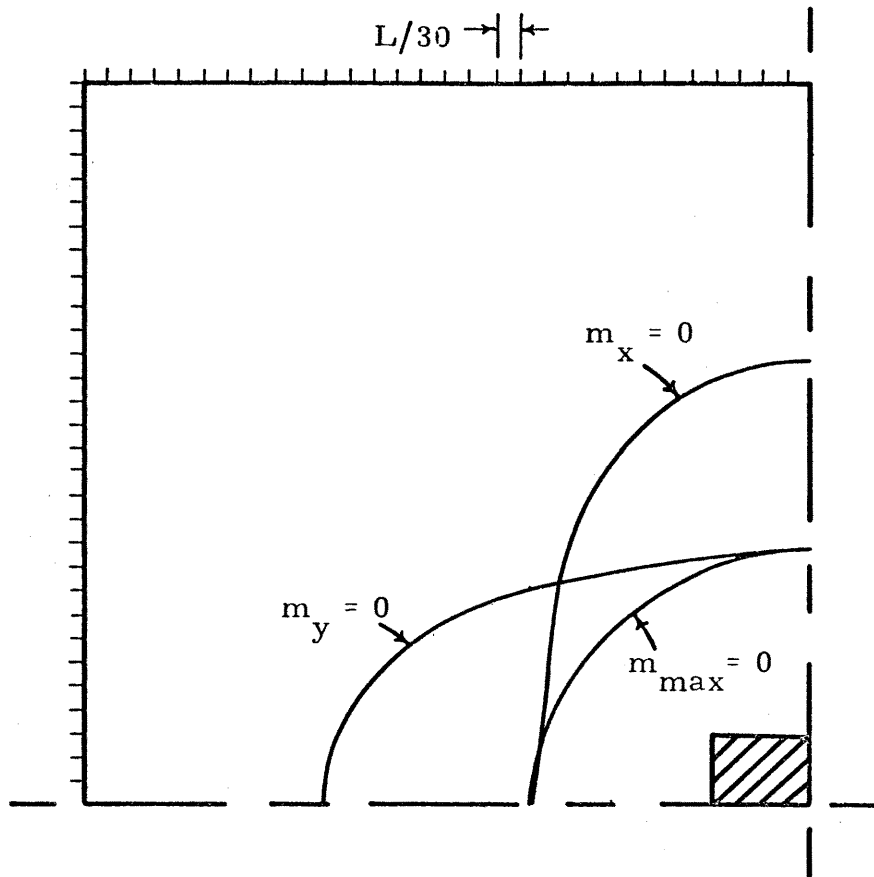


Fig. 4.14 Lines of Contraflexure Around  
a 16''x12'' Column  
in the Specimen

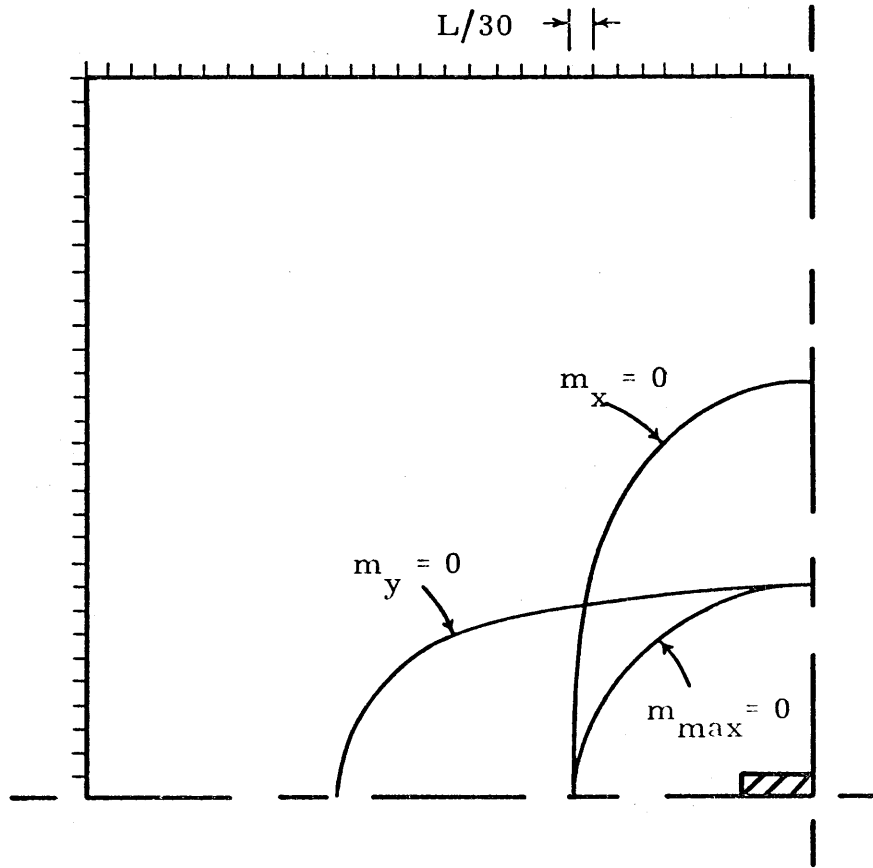


Fig. 4.15 Lines of Contraflexure Around  
a 12''x4'' Column  
in the Specimen

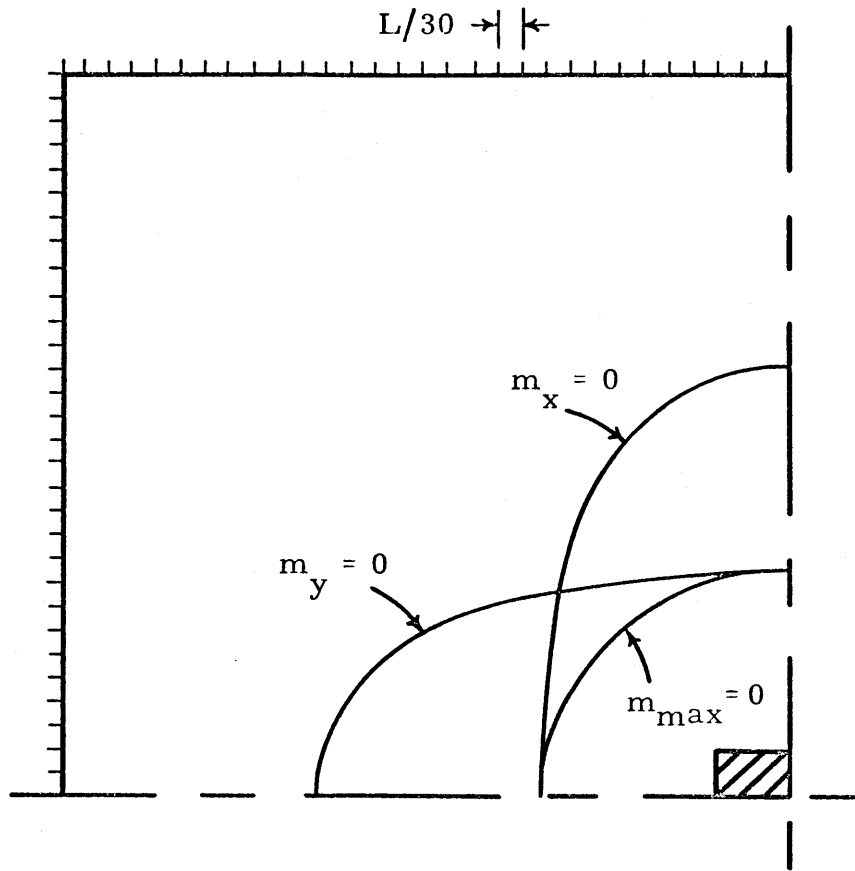


Fig. 4.16 Lines of Contraflexure Around  
a 12''x8'' Column  
in the Specimen



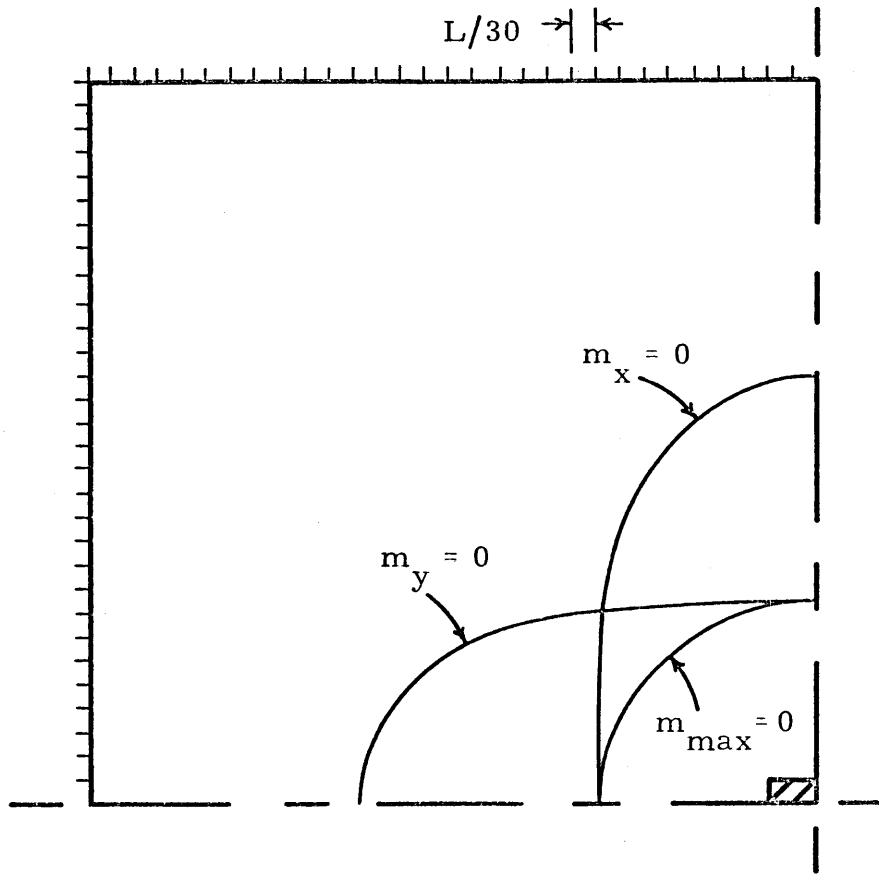


Fig. 4.17 Lines of Contraflexure Around  
a 8"x4" Center Column  
in the Specimen

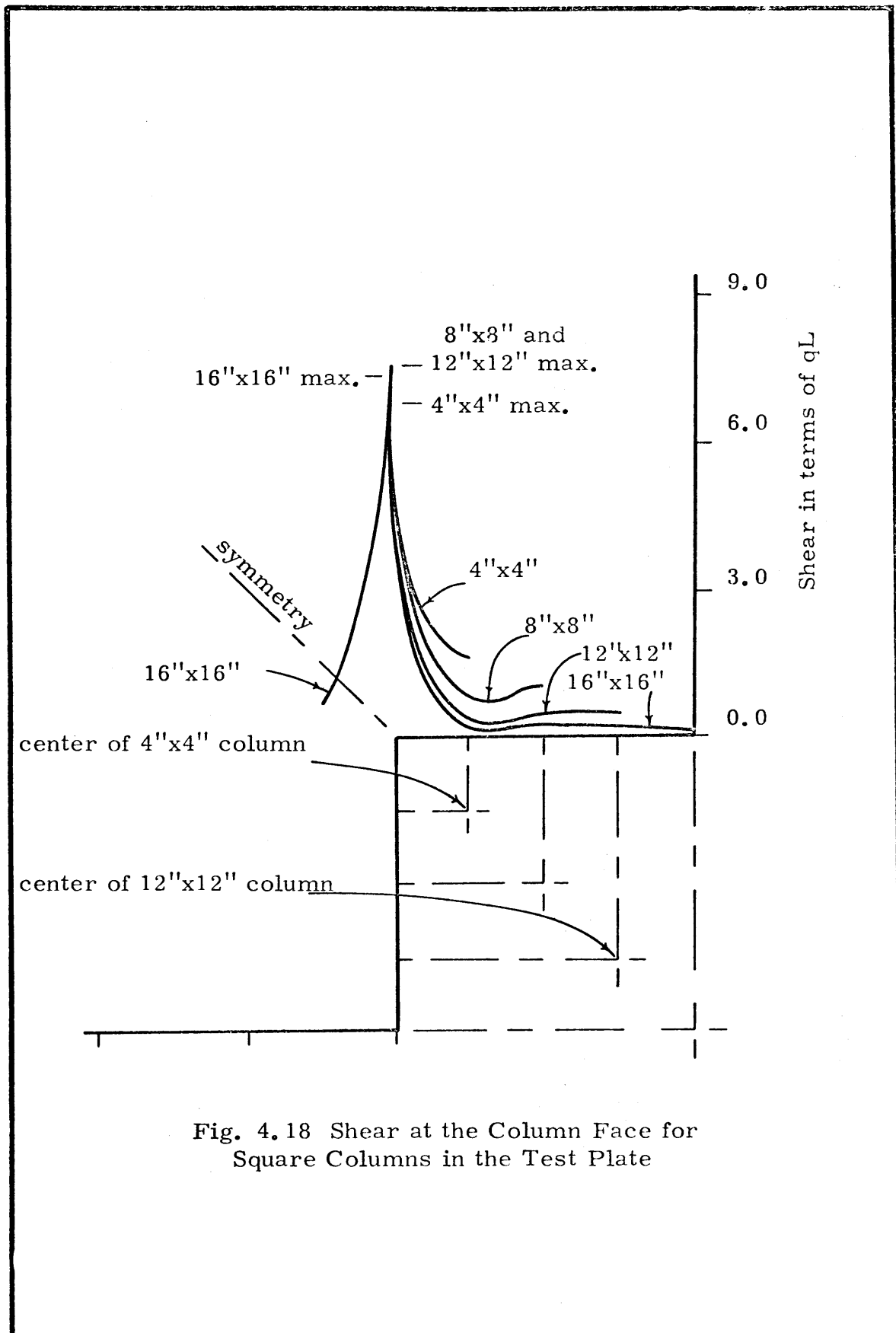


Fig. 4.18 Shear at the Column Face for Square Columns in the Test Plate

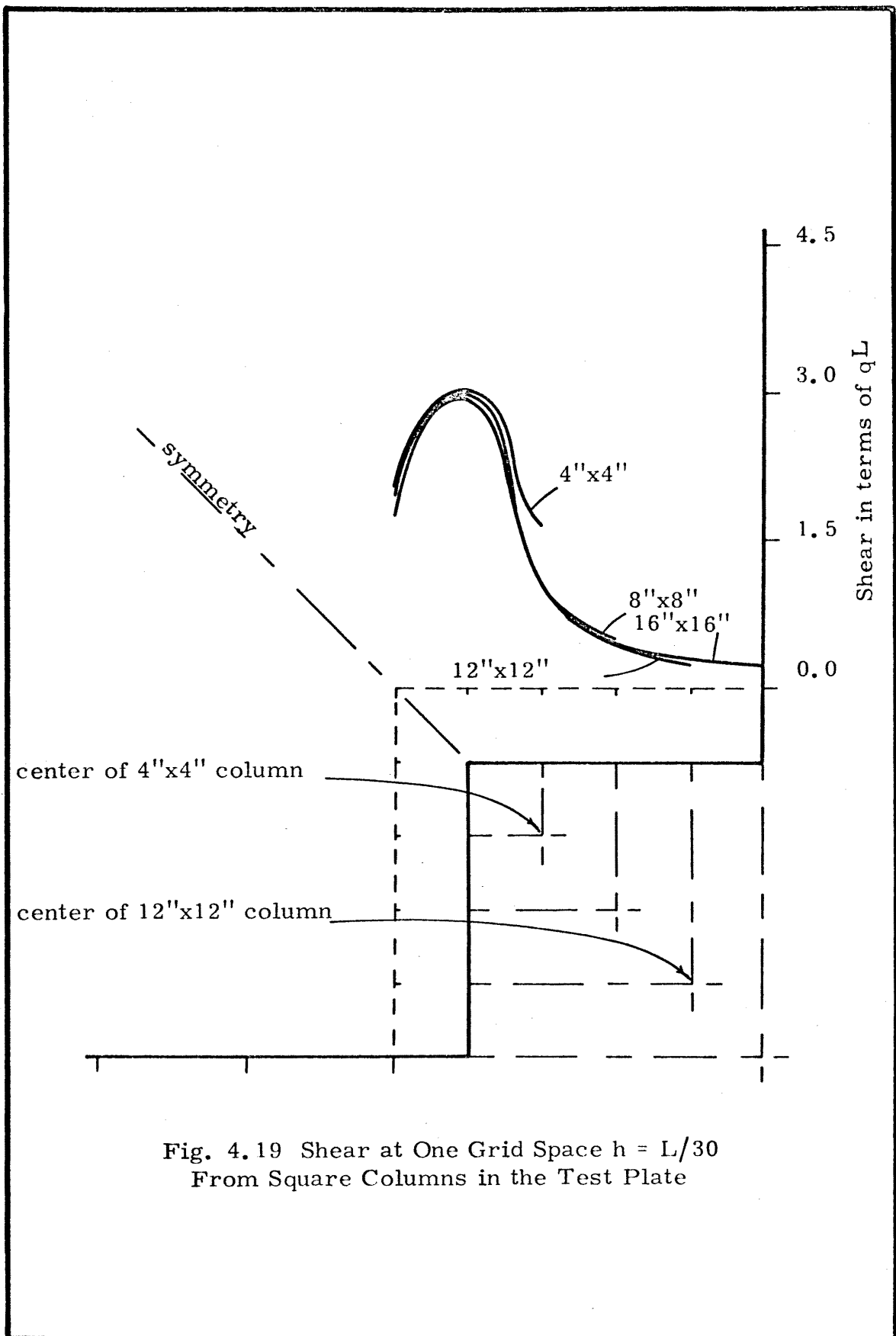


Fig. 4.19 Shear at One Grid Space  $h = L/30$   
From Square Columns in the Test Plate

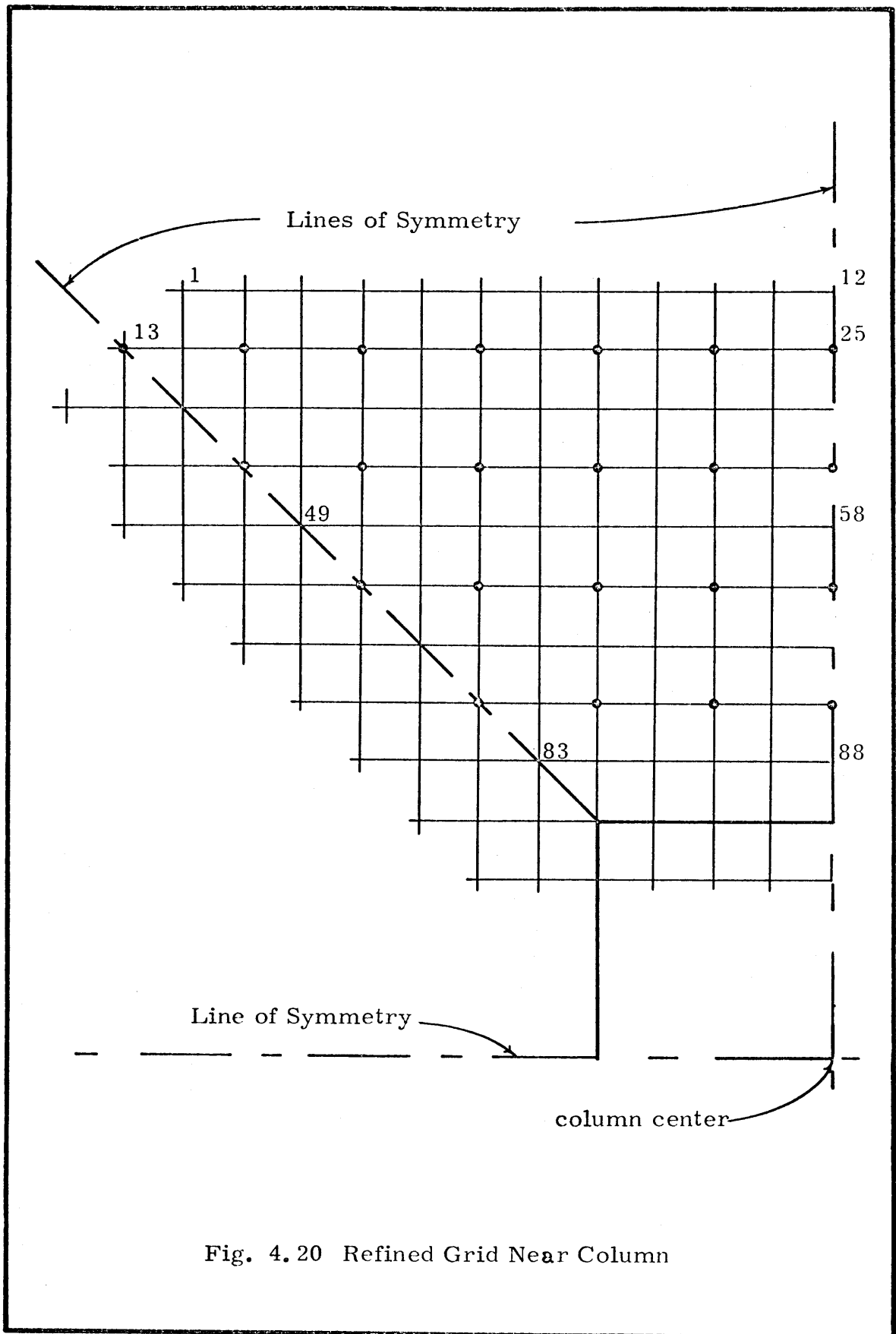


Fig. 4.20 Refined Grid Near Column

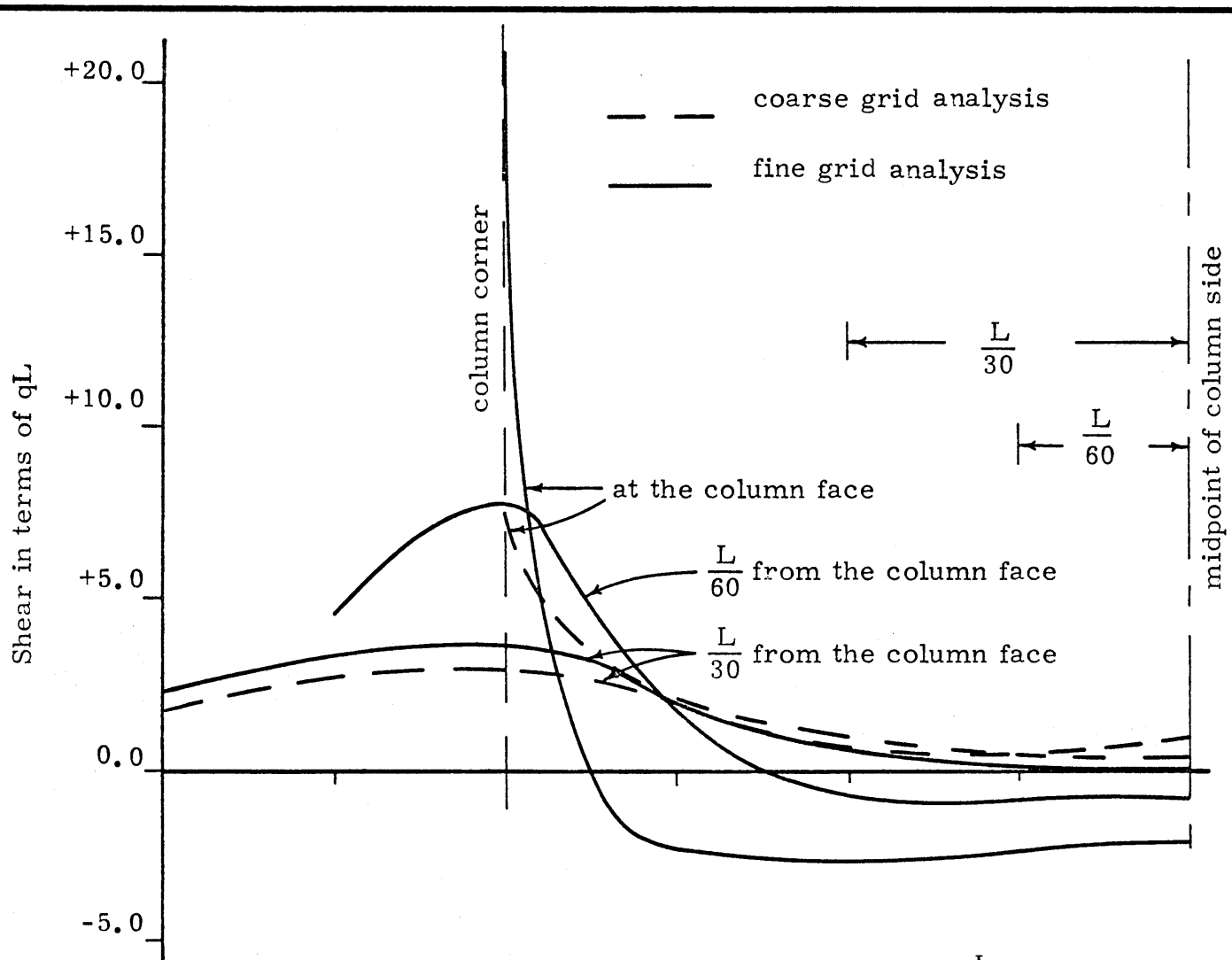


Fig. 4.21 Shear at the Column Face and at  $h = \frac{L}{30}$  from the Column Face for the Coarse and Fine Grid

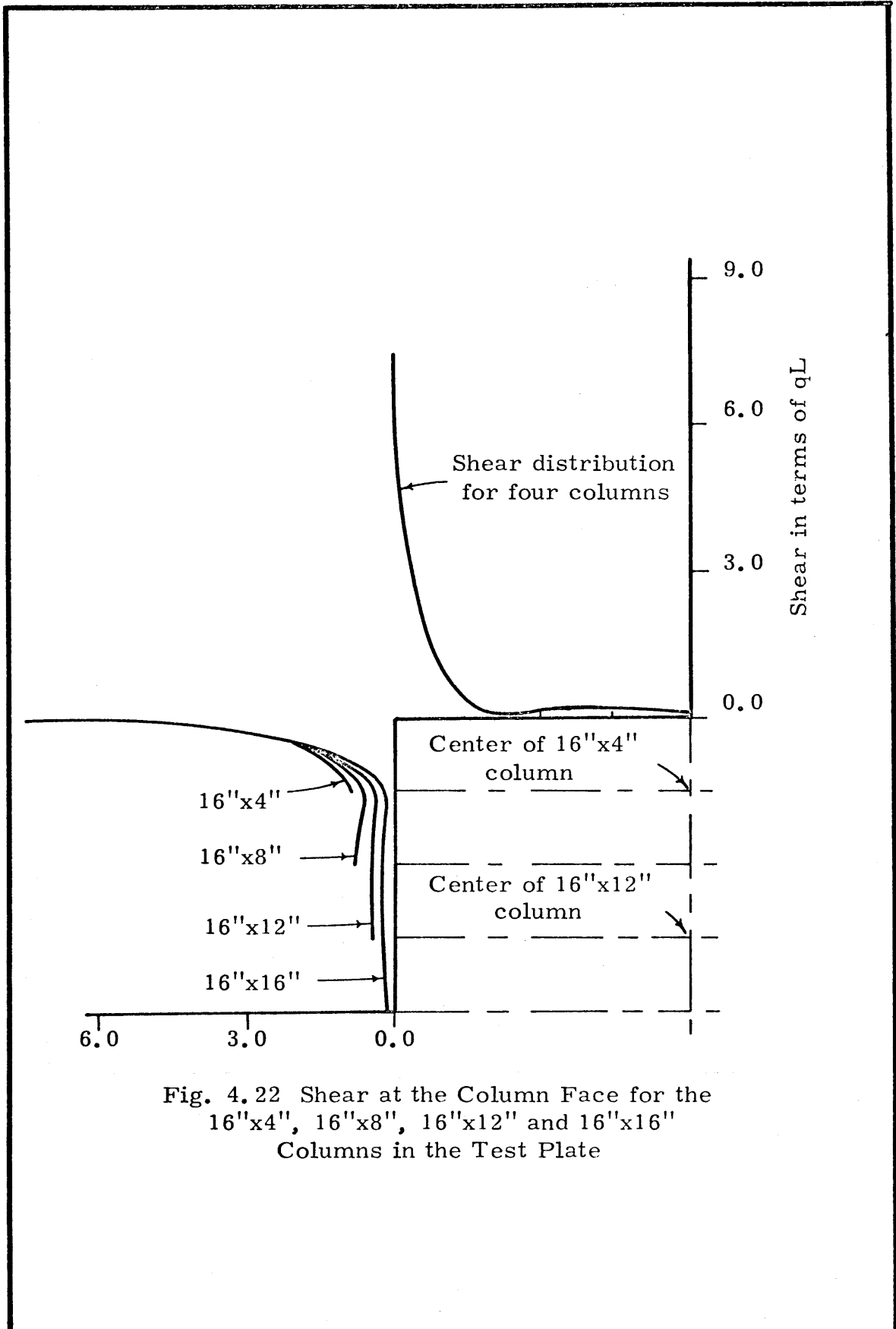


Fig. 4.22 Shear at the Column Face for the 16''x4'', 16''x8'', 16''x12'' and 16''x16'' Columns in the Test Plate

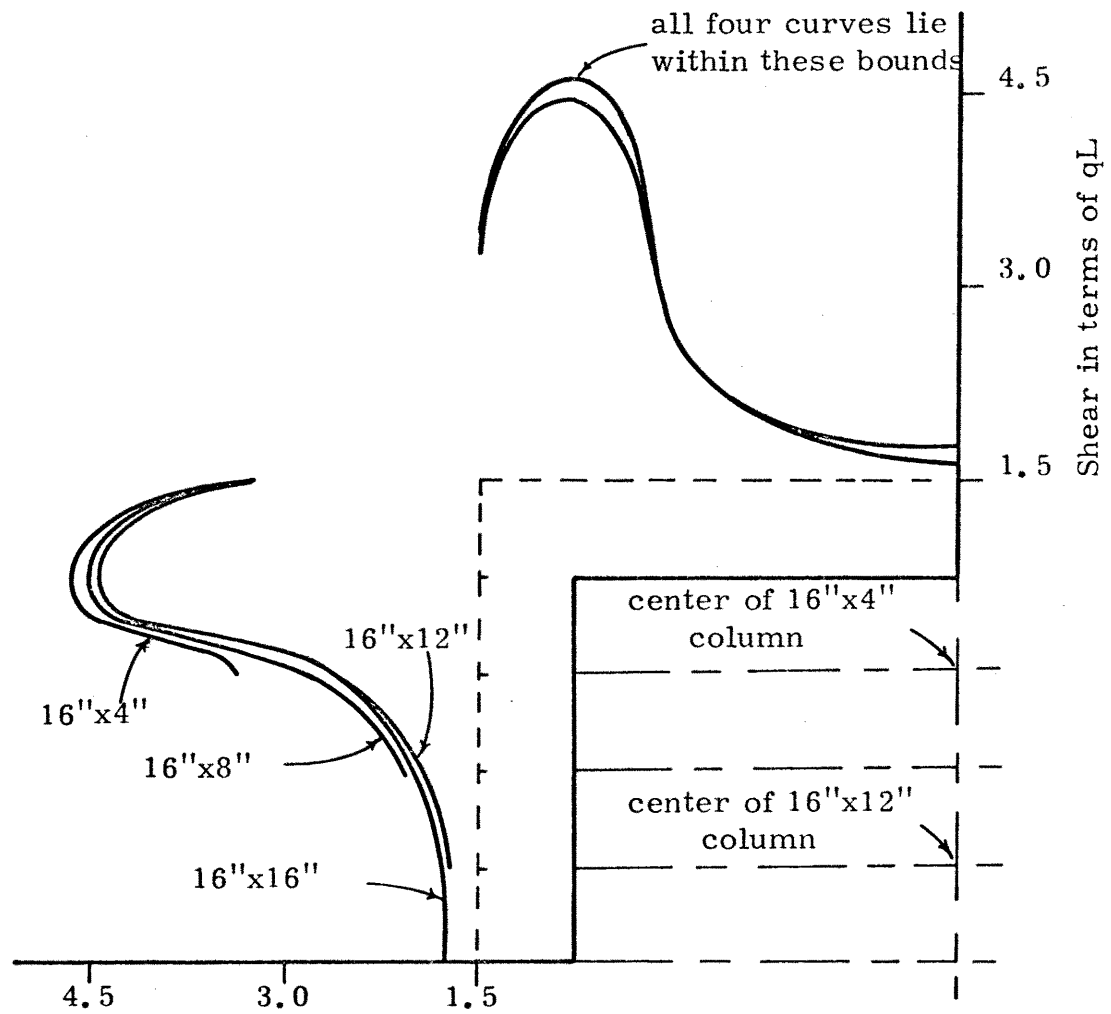


Fig. 4.23 Shear at One Grid Space from the Column for the 16"x4", 16"x8", 16"x12" and 16"x16" Columns

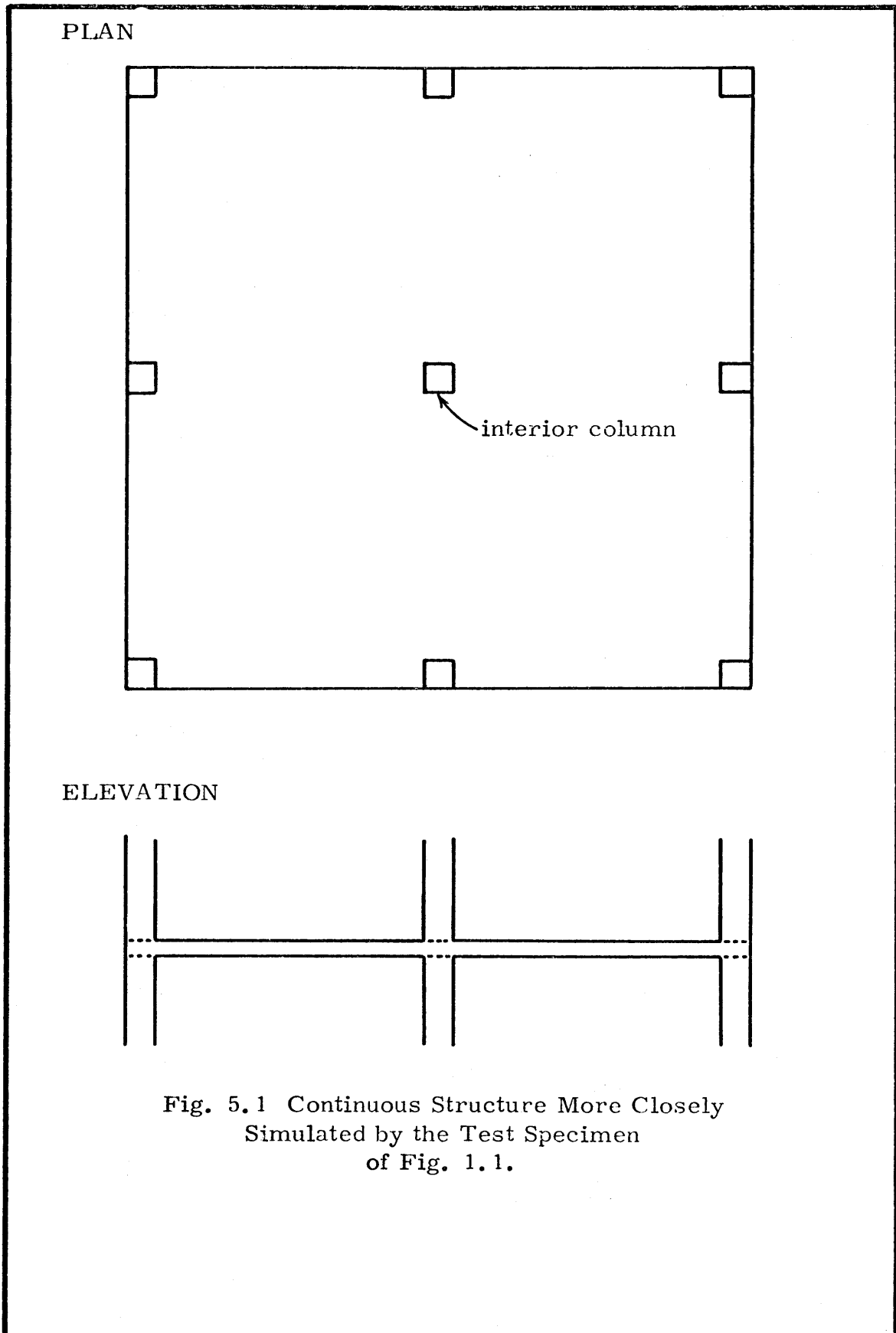


Fig. 5.1 Continuous Structure More Closely  
Simulated by the Test Specimen  
of Fig. 1.1.



## APPENDIX A

### SOLUTION OF SIMULTANEOUS EQUATIONS USING THE GAUSS ELIMINATION TECHNIQUE

#### A.1 Introductory Remarks

The set of up to 1021 simultaneous, deflection equations for the test plate were solved using a Gauss elimination and back-substitution technique. This method was selected because of its simplicity, reliability and adaptability to large, unsymmetrical, ill-conditioned matrices (12)(13). The general theory of Gauss elimination and back-substitution is explained in Section A.2. A general description and flow diagram of the algorithm written is given in Section A.3. The solution technique described here was combined with an equation generating routine to obtain program CSUPLT which actually generates and solves the deflection equations for the plate analyses.

#### A.2 Gauss Elimination and Back-Substitution

The Gauss elimination technique is a procedure for converting a general matrix into an upper-triangular matrix (one in which all elements below the main diagonal are zero). The procedure is demonstrated using the three simultaneous equations A.1 written in matrix form.

$$\begin{bmatrix} A_{11} & A_{12} & A_{13} \\ A_{21} & A_{22} & A_{23} \\ A_{31} & A_{32} & A_{33} \end{bmatrix} \begin{bmatrix} X_1 \\ X_2 \\ X_3 \end{bmatrix} = \begin{bmatrix} C_1 \\ C_2 \\ C_3 \end{bmatrix} \quad (\text{A. 1})$$

The coefficient matrix A may be converted to an upper-triangular matrix using Gauss elimination. This is accomplished by eliminating the non-zero terms to the left of the main diagonal in each row. In row 1 there are no terms to the left of the main diagonal. In row 2 the first and only term left of the main diagonal is A<sub>21</sub>. To eliminate A<sub>21</sub> compute the ratio

$$R = \frac{A_{21}}{A_{11}} \quad (\text{A. 2})$$

Next multiply row 1 by R and subtract the product from row 2.

Note that

$$R * A_{11} = \frac{A_{21}}{A_{11}} * A_{11} = A_{21} \quad (\text{A. 3})$$

so

$$A_{21} - R * A_{11} = A_{21} - A_{21} = 0 \quad (\text{A. 4})$$

which eliminates the A<sub>21</sub> term below the diagonal. Other terms in row 2 will now be

$$A_{22} - R * A_{12} = A_{22}' \quad (\text{A. 5})$$

$$A_{23} - R * A_{13} = A_{23}' \quad (\text{A. 6})$$

$$C_2 - R * C_1 = C_2'. \quad (\text{A. 7})$$

Now the form of the matrix equation is

$$\begin{bmatrix} A_{11} & A_{12} & A_{13} \\ 0 & A_{22}' & A_{23}' \\ A_{31} & A_{32} & A_{33} \end{bmatrix} \begin{bmatrix} X_1 \\ X_2 \\ X_3 \end{bmatrix} = \begin{bmatrix} C_1 \\ C_2' \\ C_3 \end{bmatrix} \quad (\text{A. 8})$$

The same procedure is now applied to row 3 in which two elements to the left of the main diagonal need to be eliminated. Compute a new ratio R as

$$R = \frac{A_{31}}{A_{11}}. \quad (\text{A. 9})$$

Multiply row 1 by R and subtract it from row 3 to obtain

$$A_{31} - R * A_{11} = A_{31} - \frac{A_{31}}{A_{11}} * A_{11} = 0 \quad (\text{A. 10})$$

$$A_{32} - R * A_{12} = A_{32}' \quad (\text{A. 11})$$

$$A_{33} - R * A_{13} = A_{33}' \quad (\text{A. 12})$$

$$C_3 - R * C_1 = C_3' \quad (\text{A. 13})$$

The form of the matrix equation is now

$$\begin{bmatrix} A_{11} & A_{12} & A_{13} \\ 0 & A_{22}' & A_{23}' \\ 0 & A_{32}' & A_{33}' \end{bmatrix} \begin{bmatrix} X_1 \\ X_2 \\ X_3 \end{bmatrix} = \begin{bmatrix} C_1 \\ C_2' \\ C_3' \end{bmatrix}. \quad (\text{A. 14})$$

To eliminate term  $A_{32}'$  a new R is computed as

$$R = \frac{A_{32}'}{A_{22}'}. \quad (\text{A. 15})$$

Multiply row 2 by R and subtract the product from row 3.

$$A32' - R * A22' = A32' - \frac{A32'}{A22'} * A22' = 0 \quad (\text{A. 16})$$

$$A33' - R * A23' = A33'' \quad (\text{A. 17})$$

$$C3' - R * C2' = C3'' \quad (\text{A. 18})$$

The form of the equations is now

$$\begin{bmatrix} A11 & A12 & A13 \\ 0 & A22' & A23' \\ 0 & 0 & A33'' \end{bmatrix} \begin{bmatrix} X1 \\ X2 \\ X3 \end{bmatrix} = \begin{bmatrix} C1 \\ C2' \\ C3'' \end{bmatrix} . \quad (\text{A. 19})$$

The Gauss elimination has now been performed on this set of equations and the coefficient matrix A has been upper-triangularized. Note the solution vector X remains unchanged during the elimination.

Back-substitution is now used to solve for the X vector.

Starting with the last row

$$X3 = \frac{C3''}{A33''} \quad (\text{A. 20})$$

Then with X3 known

$$X2 = \frac{C2' - A23' * X3}{A22'} \quad (\text{A. 21})$$

With X2 and X3 known

$$X1 = \frac{C1 - A12 * X2 - A13 * X3}{A11} \quad (\text{A. 22})$$

This methodical technique is readily adaptable to machine calculations and can be used to solve thousands of equations as well as the three equations described above.

If a diagonal term of zero is encountered, in row 2 for example, during the elimination of the term  $A_{32}'$  the ratio  $R$  of equation A.15 will be undefined. In this situation rows 2 and 3 will be switched which, with  $A_{22}' = 0$ , will change the form of equation A.14 to

$$\begin{bmatrix} A_{11} & A_{12} & A_{13} \\ 0 & A_{32}' & A_{33}' \\ 0 & 0 & A_{23}' \end{bmatrix} \begin{bmatrix} X_1 \\ X_3 \\ X_2 \end{bmatrix} = \begin{bmatrix} C_1 \\ C_3' \\ C_2' \end{bmatrix}. \quad (\text{A. 23})$$

and the upper-triangularization is completed in this particular case.

### A. 3 General Description of Algorithm GASTAP for Solving Simultaneous Equations

The simultaneous equation solver GASTAP (GAuSs elimination using TAPE storage) uses the technique of Gauss elimination combined with back-substitution and scratch tape storage in the solution of large, unsymmetrically banded matrices. It was written in Fortran IV for use on the Control Data Corporation Model 6400 Computer with 32K storage of which 27K is available. A sliding block technique is used in the solution of large sets of equations. The coefficient matrix  $A$  is dimensioned (96, 179) in the main core storage of the computer so that band widths up to about 161 may be used. The first set of equations read into core goes into  $A$  and the terms to the left of the main diagonal are eliminated. Coefficients from the upper rows of  $A$  and their corresponding constant terms are then written on tape leaving a number of equations (equal to the band

width divided by two) in the lower part of A. These equations are then transferred up the diagonal to the upper rows and more equations are read into the lower rows of A where the terms to the left of the main diagonal are then eliminated. This process continues until the whole matrix is upper triangularized, stored on tape and the A matrix in core is zeroed. Then the last batch written onto tape is read off the tape and back-substitution is performed for each equation obtaining part of the solution vector. Each batch is read off the tape and back-substitution is performed until the whole solution vector is obtained.

The amount of computer time required to obtain the solution to a set of simultaneous equations is dependent partly, of course, on the number of equations being solved. The band width of the coefficient matrix actually is the major determining factor in computer time used. One thousand equations with a coefficient matrix band width of three elements may be solved in a few seconds whereas the same number of equations with a coefficient matrix band width of one hundred twenty-nine may require two or three minutes solution time. Precision of this solution was checked by computing deflections for all the test plates which contained square center columns. These particular plates contained a diagonal line of symmetry which was not used as a boundary in generating the deflection equations. The deflections on opposite sides of this line of symmetry were checked and found to be equal or symmetrical within one percent. It should

be noted that some error is to be expected in the operator equations which describe a finite approximation.

A general flow diagram of GASTAP is given in Fig. A.1

#### A.4 Program CSUPLT--Generation and Solution of the Deflection Equations for the Test Plate

The program CSUPLT (Colorado State University PLaTe) generates and solves the deflection equations for the test plate. It is simply an extension of the basic equation solver GASTAP. The program sequentially passes from point to point on the grid, from west to east and north to south, checks the boundary conditions and node point numbering and writes the correct deflection equation for each node point on the grid (Step A, Fig. A.1). The variables considered in these equations are the edge beam flexural and torsional rigidities, Poisson's ratio of the plate material, and the column size which alters the node point numbering in the portion of the slab west of the column.

The solution of these equations is obtained using the GASTAP algorithm. The values of deflection are output on punch cards along with all values describing plate and beam properties and in particular constant indexes which describe the node point numbering and plate geometry as affected by the column size. This deck of punch card output is used directly as the input data deck for program SHRMOM which computes the shears and moments in the plate.

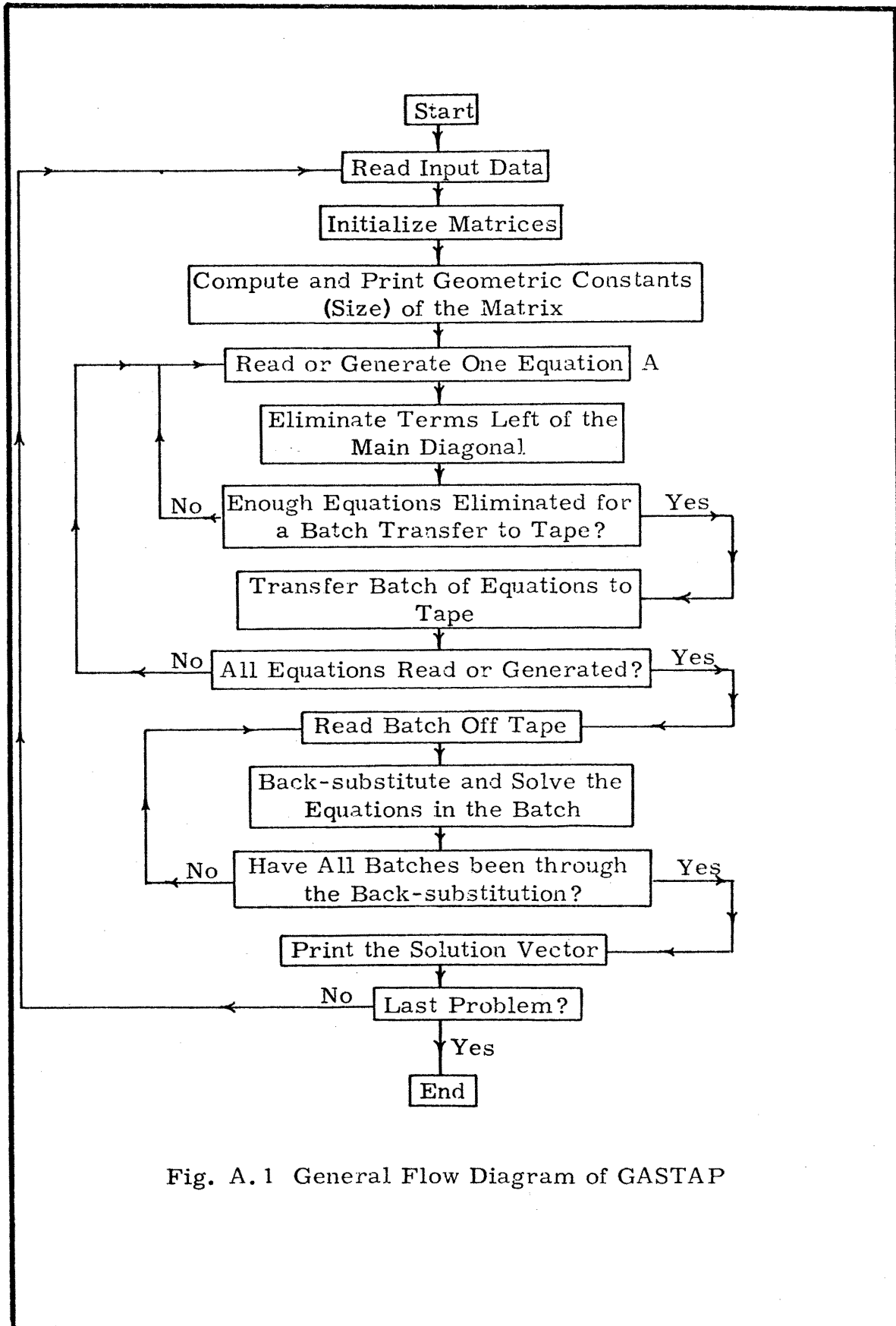


Fig. A.1 General Flow Diagram of GASTAP



## APPENDIX B

### PROGRAM SHRMOM--COMPUTATION OF SHEAR AND MOMENT IN THE TEST PLATE

The program SHRMOM (SHeaR and MOMent) computes the shears and moments in the test structure. The punch card output of CSUPLT is used as the total input data deck for SHRMOM. Shear forces at the face of the column, at  $h = L/30$  from the face of the column, and at the corner point support are computed. Two checks are then made of the static equilibrium of vertical forces on the plate. First, the total shear force at the face of the column and the shear force at the corner point support are summed. This sum should equal the load down on the quarter plate excluding that acting directly on the column. Second, the total shear force at  $h = L/30$  from the column face and the shear force at the corner point support are summed. This sum should equal the load acting on the plate excluding that acting directly on the column and within  $h = L/30$  from the column face. These calculations are made to check the validity of the shear force computed at the column and at  $h$  from the column.

Orthogonal moments, the twisting moment, principal moments and their orientation are computed for each node point in a wide area around the column. Using this information the lines of contraflexure may be drawn.

The program is written in FORTRAN EXTENDED language for use with the SCOPE operating system on the Control Data Corporation Model 6400 computer at Colorado State University. Total solution time for one test structure is about 210 seconds central memory time using the SCOPE operating system. Using the NCAR operating system solution time is 380 seconds central memory time.